Bio-Design and Manufacturing (2022) 5:556–579
https://doi.org/10.1007/s42242-022-00182-7

REVIEW

Application of additively manufactured 3D scaffolds for bone cancer treatment: a review

Yanhao Hou[1] · Weiguang Wang[1] · Paulo Bartolo[1,2]

Received: 3 July 2021 / Accepted: 28 December 2021 / Published online: 7 March 2022

Abstract

Bone cancer is a critical health problem on a global scale, and the associated huge clinical and economic burdens are still rising. Although many clinical approaches are currently used for bone cancer treatment, these methods usually affect the normal body functions and thus present significant limitations. Meanwhile, advanced materials and additive manufacturing have opened up promising avenues for the development of new strategies targeting both bone cancer treatment and post-treatment bone regeneration. This paper presents a comprehensive review of bone cancer and its current treatment methods, particularly focusing on a number of advanced strategies such as scaffolds based on advanced functional materials, drug-loaded scaffolds, and scaffolds for photothermal/magnetothermal therapy. Finally, the main research challenges and future perspectives are elaborated.

Keywords Additive manufacturing · Biomanufacturing · Bone cancer · Implants · Tissue engineering

Introduction

According to the World Health Organization (WHO), cancer caused 10 million deaths in 2020 with 19.3 million new cases detected in the same year [1]. The total annual cancer-related economic costs in the USA added up to $183 billion for 2015 [2], and €199 billion in Europe for 2018 [3]. Bone cancer is caused by cancer cells originating in bone tissue (primary bone cancer) or metastasized from other primary tumor areas to bone tissue (metastatic bone cancer) [4]. Around 700,000 new primary bone cancer cases are reported each year worldwide [5, 6]. Due to the low incidence of bone cancer, its delayed diagnosis and treatment are common, leading to high mortality. More than 220,000 patients die following treatment each year, resulting in a global survival rate of around 68% [5]. Among all reported cases, osteosarcoma, Ewing sarcoma, and chondrosarcoma are the three most common primary bone cancer types, and breast, prostate, thyroid, and lung are the four regions of cancer origin with the highest bone metastasis risk [7–9].

As most solid tumors can be surgically resected, clinical surgery is normally considered as the first choice for bone cancer treatment. However, the limited regenerative capabilities of bone result in large-sized bone defects and spontaneous healing difficulties. Clinical therapies to address this problem include the use of biological grafts (autografts, allografts, and xenografts) and artificial substitutes (implants) [10, 11]. In the cases of tumors of more advanced stages, metastasis to other body regions, or unresectable ones (in regions where surgery is difficult or has high risk), chemotherapy, radiotherapy, and targeted cancer drugs are the alternative clinical approaches [12]. These methods are based on the delivery of high systemic doses of chemotherapeutics and targeted cancer drugs such as cisplatin, daunorubicin, docetaxel (DTX), doxorubicin (DOX), paclitaxel (PTX), fluorouracil (5-FU), and mifamurtide [13]. However, such agents are often associated with potential side effects including kidney toxicity (cisplatin) [14], myocardial and cardiac toxicity (DOX) [15–17], and neurotoxicity (PTX) [18, 19]. The delivery of these therapeutics via nanoparticle carriers (e.g., polymers, lipids, silica, iron oxide,

✉ Weiguang Wang
weiguang.wang@manchester.ac.uk

✉ Paulo Bartolo
paulojorge.dasilvabartolo@manchester.ac.uk;
pbartolo@ntu.edu.sg

1 Department of Mechanical, Aerospace and Civil Engineering, School of Engineering, Faculty of Science and Engineering, The University of Manchester, Manchester M13 9PL, UK

2 Singapore Center for 3D Printing, School of Mechanical and Aerospace Engineering, Nanyang Technological University, Singapore, Singapore

and gold) is a viable approach to overcome these limitations [20, 21]. Other strategies are aimed at releasing therapeutics near the cancer regions in response to environmental changes (e.g., temperature or pH value), thus reducing the risks of using high doses [20]. However, therapeutics still enter the systemic circulation, and the clinical problems related to large tissue defects following tumor resections remain [22].

Since the 1970s, different strategies have been proposed in combination with the use of implants, including delivering antibiotics to prevent bacterial infections and biofilm formation [23, 24], and adding molecules such as growth factors [25, 26]. Clinical implants can also be loaded with chemotherapeutics for local cancer treatment applications, combining the advantages of post-operative clinical implants and chemotherapy [27, 28]. One of the first such examples is Gliadel® Wafer (Eisai Inc., Japan), a drug-loaded implant for malignant glioma treatment [29]. Implants made from functional materials and those containing chemotherapeutics and targeted cancer drugs, implanted in the resected cancer region, represent a novel and promising approach. In this case, the implant should not only provide mechanical support, but also promote tissue repair, prevent cancer recurrence, and improve patient outcomes [30]. Another strategy is based on the use of implants sensitive to external electromagnetic radiation for photothermal/magnetothermal therapy. These implants contain photo-sensitizers or magneto-sensitizers; they are placed on the site of the lesion, excited with a near-infrared (NIR) radiation or a magnetic field, and, as a consequence, release heat. As cancer cells have a lower heat tolerance than normal cells, the induced heat from the implants leads to irreversible protein denaturation, cell membrane damage, and progressive apoptosis [31]. Contrary to conventional treatments, local photothermal/magnetothermal therapies can selectively and effectively eliminate cancer cells without damaging the surrounding normal cells [32]. All of these approaches have been considered for the treatment of both primary bone cancer and/or metastatic bone cancer.

Due to the limitations of conventional bone cancer therapies, new and more effective methods are being investigated, and in turn several advanced approaches have been proposed using implants for local sustained treatment and photothermal/magnetothermal therapy. These implants are fabricated using additive manufacturing to achieve high customization, high reproducibility, and relatively low fabrication costs. These novel therapeutic methods seem to represent suitable approaches for future bone cancer treatment and post-treatment bone regeneration. This review discusses the limitations of the current clinical treatment methods of bone cancer and provides a detailed review of novel treatment approaches using additively manufactured 3D clinical implants as local cancer treatment substrates. The key research challenges are also discussed.

Bone cancer and corresponding treatments

Bone makes up the human skeleton, which supports, moves, and protects the human body and the internal organs. It also provides stable points for muscles to attach, stores essential nutrients and minerals critical for different body functions [33], and produces lipids and blood cells [34]. Bone cells (osteoblasts, osteocytes, and osteoclasts) are responsible for new bone formation, mineralization, and bone destruction [35, 36]. As a load-bearing tissue, the bone is continuously exposed to shear and compressive forces, which further modulate bone homeostasis (Fig. 1a) [37]. The connection between the bone niche and the etiology of primary bone cancer has not been clearly defined. However, research has indicated that some acquired and congenital factors can increase the incidence of primary bone cancer, and regular inspections are critical to prevent the onset of bone cancer [37].

Bone cancer types

Primary bone cancer

According to the WHO, primary bone cancers can be classified into chondrogenic tumors, miscellaneous tumors, notochordal tumors, osteogenic tumors, vascular tumors, and other malignant mesenchymal tumors [38].

Osteosarcoma is one of the most common of primary bone cancers, with around 150 new cases each year in the UK [39]. The incidence ratio between males and females is 1.4:1 and the two age groups with peak incidence are adolescents aged 10–19 years and adults above 60 years of age [40, 41]. Osteosarcoma is more common in adolescence in Afro-Caribbeans and Caucasian adults [42]. Younger patients have a significantly higher 5-year survival rate than patients aged over 40 (53% in the case of patients below 40, and 22% in the case of patients over 40) [43]. The high-incidence regions include the metaphysis of long bones such as the ankle and knee joint, affecting the femur (40%, usually distal), tibia (20%), humerus (10%), and pelvis (8%) [42]. The etiology of osteosarcoma is still unclear. However, it is widely accepted that loading stresses and rapid bone growth, which can be attributed to the pubertal growth spurt and regions in the metaphysis of long bones, cause DNA mutations leading to disease [12, 44].

Ewing sarcoma, another common primary bone cancer, exhibits different degrees of neuroectodermal differentiation [45]. It has higher incidence in males than females (1.5:1) [46]. Around 80% of Ewing sarcoma patients are children and adolescents, with a median age of around 15 years [12]. Whites have a higher incidence rate than Asians and Blacks [12]. Its survival rate highly depends on the metastasis status, with around 20–25% of diagnosed cases showing clinically

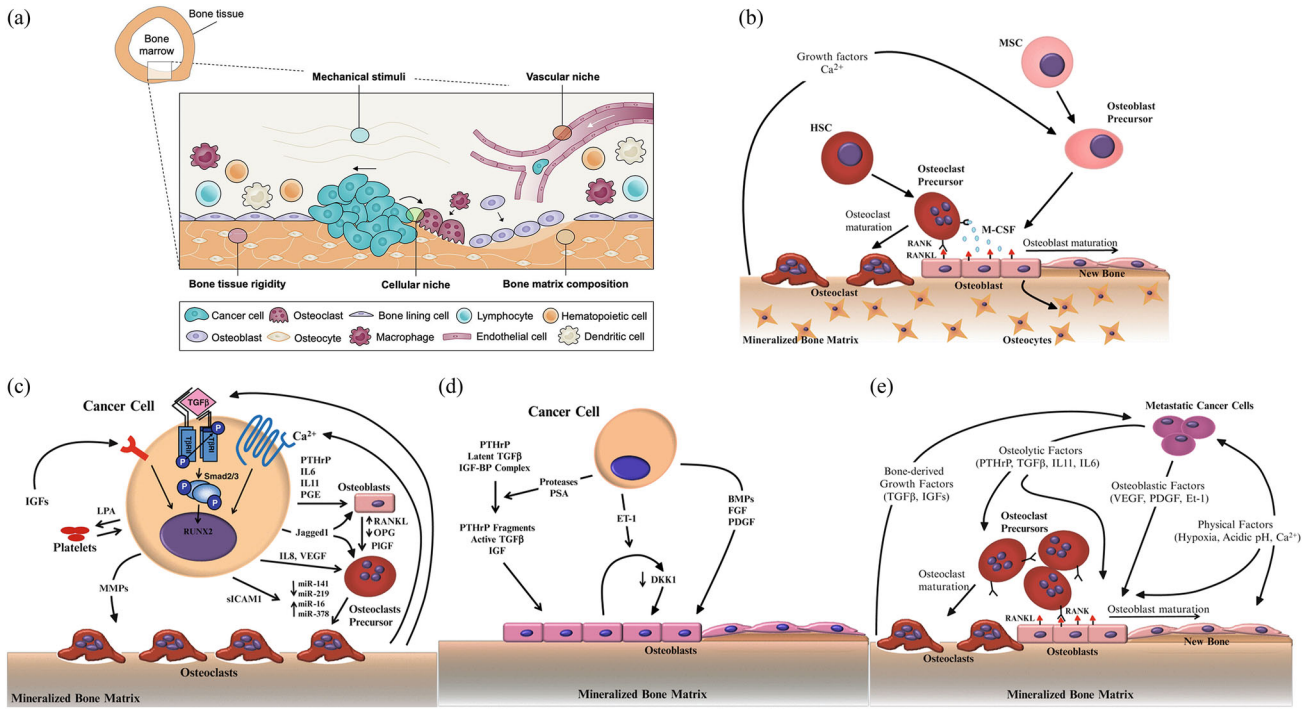

Fig. 1 **a** Cell–cell and cell–matrix interactions in a multifactorial bone cancer niche (Reproduced from [37], Copyright 2019, with permission from Elsevier). The mechanism of **b** normal bone remodeling, **c** osteolytic bone metastasis, **d** osteoblastic bone metastasis, and **e** vicious cycle (Reproduced from [56], Copyright 2016, with permission from Springer Nature)

detectable metastasis. In the case of localized tumors, the 5-year survival rate is around 50–60%, and it significantly decreases to around 20% in the case of metastatic sarcoma [47]. Approximately 60% of Ewing sarcoma cases start from flat bones and 40% of them affect the metaphysis of long bones [45, 48]. This type of primary bone cancer typically occurs in the legs, pelvis, ribs, and vertebral column [12]. Ewing sarcoma is a non-complex karyotype sarcoma, as specific gene fusion proteins (e.g., EWS/FLI1) drive tumor oncogenesis [7, 42]. It can be characterized by a variety of chromosomal translocations, but 85–90% of cases correspond to the t(11;22)(q24;q12) chromosomal translocation, involving the Ewing sarcoma gene on chromosome 22 and the Friend leukemia virus integration site 1 (FLI1) gene on chromosome 11 [44, 49].

Due to the ageing population, chondrosarcoma is the most common primary bone cancer in many countries, with around 180 new cases in the UK each year [44]. There are no significant differences in the incidence between genders and ethnicities, while adults aged between 30 to 60 have a higher risk of incidence [41]. Long bones, such as pelvis and ribs (45%), ilium (20%), femur (15%), and humerus (10%), have a higher incidence risk than flat bones like the scapula [50]. Similar to other bone cancers, chondrosarcoma can be characterized by marked heterogeneity at the histological, genetic, and epigenetic levels [7].

Metastatic bone cancer

Bone tissue is one of the most frequent sites of cancer metastasis, third to the lung and the liver [51]. Metastatic bone cancer is usually manifested in severe pain, impaired mobility, pathologic fractures, spinal cord compression, bone marrow aplasia, and hypercalcemia [52]. Cancer cells from the primary cancer regions can be relocated through the bloodstream and the lymphatic system to the bone. Briefly, the metastasis of cancer cells includes the loss of intercellular cohesion, cell migration, angiogenesis, access to systemic circulation, survival in circulation, the evasion of local immune responses, and growth at distant organs [53, 54]. Vascular adhesion and extravasation, microenvironmental support, and epithelial-mesenchymal transition are the critical factors affecting metastasis [51]. The metastasis of cancer to bone usually means short-term prognosis for patients, indicating that cancer can be rarely cured, whereas the growth process can often be slowed down (Table 1).

According to the interference mechanism with normal bone remodeling, bone metastases are classified as osteolytic, osteoblastic, and a combination of both (mixed mechanism) (Figs. 1b–1d) [56]. Osteolytic bone metastasis, characterized by the destruction of normal bone, is commonly present in multiple myeloma, melanoma, non-small cell lung cancer,

Table 1 Relative incidence of bone metastasis and median survival from time of diagnosis in different primary cancer types [9, 55]

Primary cancer type	Breast cancer	Prostate cancer	Thyroid cancer	Lung cancer	Bladder cancer	Renal cell carcinoma	Melanoma
Relative incidence of bone metastasis	65–75%	65–75%	60%	30–40%	40%	20–25%	14–45%
Median survival from time of diagnosis	19–25 months	12–53 months	48 months	6–7 months	6–9 months	12 months	6 months

non-Hodgkin lymphoma, renal cell carcinoma, thyroid cancer, Langerhans-cell histiocytosis, and most breast cancers [51, 57–59]. Osteoblastic bone metastasis, featured by the deposition of new bone, is commonly present in carcinoid, prostate cancer, small cell lung cancer, Hodgkin lymphoma, and medulloblastoma [51, 57–59]. The mixed mechanism, which includes both osteolytic and osteoblastic lesions, or individual metastasis with both osteolytic and osteoblastic components, is commonly present in breast cancer, gastrointestinal cancers, and squamous cancers [51, 57–59]. Both osteolytic and osteoblastic bone metastases promote a vicious cycle involving cancer cells, osteoblasts, osteoclasts, and the bone matrix (Fig. 1e) [56, 60]. In the case of osteolytic bone metastasis, osteoclasts resorb the bone and release growth factors and calcium from the mineralized bone matrix [61]. The released growth factors and calcium stimulate the proliferation of cancer cells, produce high levels of parathyroid hormone-related protein, further inducing osteoclastogenesis and bone resorption [56]. In the case of osteoblastic bone metastasis, cancer cells release factors that promote osteoblast proliferation and differentiation, as well as new bone deposition. Subsequently, osteoblasts release growth factors that promote bone tumor growth [62–64].

Current bone cancer treatment approaches

Depending on the type, location and extension of cancer and the overall health condition of patients, the current clinical treatment strategies of bone cancer comprise surgery, chemotherapy, radiotherapy, targeted therapy, immunotherapy, and the combinations of these methods (Table 2). Unlike primary bone cancer that usually has defined treatment guidelines [12], the treatment of metastatic bone cancer generally requires case-by-case consultation by doctors. All of the different treatment approaches may be applied depending on the type of primary tumor, the bones that primary cancer has invaded, the extent of damage to the bones, the types of treatment already applied, and the overall health conditions of affected patients [65]. As cancer metastasis to bone usually corresponds to terminal cancer stages and short-term prognosis, treatments focus on pain relief, preventing complications and improving the life quality [65].

Table 2 Common primary bone cancer types, corresponding treatments, and 5-year survival rates [7, 12, 44, 46, 66]

Bone cancer type	Corresponding treatment	Five-year survival rate
Osteosarcoma	Chemotherapy, surgery	60–70% (normal), 30% (with lung metastasis), 90% (grade I), 40% (grade II) and 25% (grade III)
Ewing sarcoma	Chemotherapy, radiotherapy, and surgery	66% (normal), 20% (poor responders), 40% (central) and 60% (extremities)
Chondrosarcoma	Surgery	77% (overall), 90% (grade I) and 29% (grade III)

Surgery

Surgery, an important bone cancer treatment method, is usually combined with other approaches [67]. The primary goal of surgery is to completely resect the cancer region, and the secondary goal is to keep the limb as functional as possible. Therefore, limb-sparing surgery (LSS) is always the first approach considered to avoid completely removing an affected body part. If the tumor located on the bone does not affect the body function, such as ribs, the bones can be directly removed. In other cases, tumors will be removed and replaced by bones from a bone bank, autologous bones, or an artificial implant [12, 67]. In these cases, the surgical area is often larger than the cancer region to achieve the full removal of the tumor and to prevent its recurrence [68]. In some rare cases (e.g., extracorporeal irradiation), bones will be taken out, irradiated, and returned to the patient's body [12]. Although the LSS procedure allows for better functional results than amputation, up to 10% of patients still need to have a limb permanently removed (e.g., in cases of large tumors size, critical nerve involvement, and complicated cancer region locations) [67, 69].

As the growth of cancer region is a process occurring from inside out, the surrounding tissue is compressed and forms a pseudocapsule at the interface between the cancer region and the normal tissue, and pseudopods of the tumor extend into this interface [70]. Thus, an adequate surgical margin (the

Table 3 Margins in surgical tumor resection [72]

Type of margin	Plane of dissection
Intralesional	Within diseased tissue of tumor
Marginal	Within reactive zone
Wide	Through normal tissue, beyond reactive zone
Radical	Extra-compartmental

boundary of removed tissue) is critical to prevent bone cancer recurrence [71]. Enneking [72, 73] described four types of surgical margin (Table 3), and the National Comprehensive Cancer Network guidelines recommend the wide local excision of bone sarcomas. Moreover, resection is often more challenging in the pelvis and spine than it is in the extremities due to the associated anatomical complexity [74].

Although LSS may allow for better functional results than amputation, the risk of post-surgical complications is three times higher, and the risk of complications after end prosthetic reconstruction is fourfold [75]. These complications can be classified as mechanical (e.g., soft tissue failure, aseptic loosening, and breakage/fracture/dislocation of the implant), non-mechanical (e.g., infection and tumor progression) and pediatric (e.g., growth arrest and joint dysplasia) [76].

Chemotherapy

Chemotherapy is an approach that uses cytotoxic drugs to suppress cancer cells to prevent them from growing and spreading in the body, and to reduce the risk of recurrence of cancer [67]. This clinical approach is mainly performed via oral and intravenous administration, while other administration methods have been also used, such as subcutaneous, intramuscular, intrathecal, and the use of skin creams [67, 77, 78]. Chemotherapy is usually combined with other treatments and can be used before surgery (neo-adjuvant chemotherapy) to decrease the risk of distant recurrence after surgery or to control the development of primary cancer [67, 78]. This treatment can also be carried out after radiotherapy or surgery (post-operative adjuvant chemotherapy) to reduce the risk of cancer recurrence [67, 78]. It can also be used individually to relieve symptoms in cases where it is impossible to fully cure the patient (palliative chemotherapy) [67, 78]. Chemotherapy is one of the most frequently used treatment approaches for non-metastatic high-grade osteosarcomas such as Ewing sarcoma, which includes treatments with neo-adjuvant chemotherapy followed by definitive local therapy and then adjuvant chemotherapy [77, 79]. However, chemotherapy is still not fully effective for other types of bone cancer such as chondrosarcoma [12, 80].

The side effects of chemotherapy can differ from patient to patient, but usually include nausea, vomiting, constipation, indigestion, insomnia, headache, anemia (by reducing the number of red blood cells that carry oxygen around the body), bruising and bleeding (by lowering the number of platelets in the blood), skin and nail changes (e.g., dryness, slight discoloration, increased sensitivity to sunlight, redness, soreness and itchyness), fatigue, hair loss, lower resistance to infections, sore mouth, loss of appetite, memory and concentration problems, sex and fertility issues [12, 80–82]. Moreover, chemotherapy presents other limitations such as difficulty of reaching cancer cells far from tumor vessels, and short half-life reducing drug bioavailability and treatment effectiveness [83–86].

Radiotherapy

Radiotherapy uses radiation to treat cancer and to reduce the risk of recurrence either in the early stage or after spreading. This treatment type is usually carried out by applying external ionizing radiation (radioactive beams at the cancer regions), radiotherapy implants (brachytherapy, implanting small pieces of radioactive metal near the cancer regions), radiotherapy injections, capsules or drinks (radioisotope therapy, oral or injected radioactive liquids), and intrabeam radiotherapy [67]. Advanced radiotherapy techniques, such as carbon ion beam radiotherapy, intraoperative radiation, and proton beam radiation, have also been proposed [87–89]. Radiotherapy can also be combined with chemotherapy or used before surgery (neo-adjuvant radiotherapy) to help reduce the cancer region and minimize the surgery area [67, 90]. Moreover, it can be applied after surgery to eliminate residual cancer cells, preventing recurrence [67, 90]. In the case of unresectable tumors or symptomatic widespread metastatic primary tumors, radiotherapy is used to relieve symptoms if full cure is not possible (palliative radiotherapy) [67, 90]. In other cases, radiotherapy can be considered as an adjunct therapy (marginal resection), or as an alternative to surgery (e.g., in difficult locations such as pelvis, spine, and chest wall) [80]. Radiotherapy is an effective method for the local control of Ewing sarcoma, but as a standalone option is not the ideal modality for primarily localized bone sarcomas [12].

The side effects of radiotherapy include sore skin (darker than normal or dry and itchy), hair loss (unlike chemotherapy, only affecting the area being treated), eating and drinking problems (e.g., sore mouth, loss of appetite, weight loss, and discomfort when swallowing), fatigue, feeling sick, diarrhea, stiff joints and muscles, sex and fertility issues, wound complications, limb-length discrepancies, joint contractures, pathologic fractures, and secondary malignancy [12]. Moreover, it was reported that even relatively low doses of radiation could increase the incidence of sarcomas induced by radiation, usually presenting a worse prognosis than those not related to radiation exposure [91, 92].

Targeted therapy

Targeted therapy inhibits the growth and spread of cancer cells by aiming at specific factors necessary for cancer development (e.g., molecules, genes, and proteins) while limiting the damage to healthy cells [4, 93, 94]. The target drugs can be classified into monoclonal antibodies, cancer growth blockers, antiangiogenics, and poly (ADP-ribose) polymerase inhibitors, and the common drugs include Avastin (Roche, Switzerland), Herceptin (Roche, Switzerland), Mabthera (Roche, Switzerland), Olaparib (AstraZeneca, UK), Mifamurtide (Takeda, Japan), and Imatinib (Novartis, Switzerland) [94–96]. Some studies have already validated targeted therapy as an effective method for treating primary bone cancer such as chondrosarcoma and chordoma [94, 96] and metastatic bone cancer secondary to breast and prostate cancers [97, 98]. However, due to the high heterogeneity of bone cancer, its targeted therapy is not as effective as surgery, chemotherapy, or radiotherapy [99, 100]. Therefore, despite some promising results, this therapy is still not the first choice of clinicians.

The most common side effects of targeted therapy include fatigue, nausea, dizziness, vomiting, increased liver enzymes, cough, constipation, and diarrhea [101].

Immunotherapy

Immunotherapy approaches include cancer vaccines, cell-based immunotherapy, immune checkpoint blockade, and cytokines [102–104]. Cancer vaccines, one of the first immunotherapies to be used for bone cancer treatment [105], use neoantigens derived from whole tumor cells, tumor cell lysates, and cancer-related peptides [106, 107]. Tumor antigen-specific T cells are activated by the major histocompatibility complex molecules of antigen-presenting cells and eventually trigger immune response [108]. Cell-based immunotherapy mainly uses tumor-infiltrating lymphocytes or cytotoxic T lymphocytes [107]. Cells are sorted from a patient, expanded and stimulated ex vivo, and transferred back to the patient [109]. Immune checkpoint blockade removes the brakes of the immune system [110]. The currently approved checkpoint blockade inhibits PD-1, CTLA-4, and PD-L1 [102]. Cytokines (e.g., interleukin-2 and interferons), the proteins that regulate the immune system, have been used for the immunotherapy of sarcomas [111]. Immunotherapy represents a clinically accepted approach to treat certain cancers (e.g., melanoma, renal cell carcinoma, prostate cancer, and lung cancer), but their limited success has been reported for bone cancer [103]. The possible reasons can be the relatively low immunogenicity of bone cancer [112, 113], difficulty in establishing bone cancer cell lines and autologous CTL [114, 115], the lack of targetable neoantigens and suitable candidate genes for a reverse immunological approach [116–118], and also that most bone cancer cells express immune checkpoint proteins contributing to their immune escape [118]. Further investigations of the bone cancer microenvironment and immunological milieu are needed to better understand the markers that predict the immune responsiveness of patients with sarcomas [103].

The main side effects of immunotherapy include diarrhea, rashes, nausea, vomiting, respiratory symptoms, and prolonged times to achieve effectiveness [102].

Advanced cancer treatment strategies based on synthetic 3D scaffolds

Advanced manufacturing technologies and novel materials opened up new routes for the development of new therapeutic strategies, namely the use of 3D scaffolds based on functional materials, drug delivery carriers, and scaffolds used as photothermal/magnetothermal therapy substrates. A particularly relevant method is the use of additive manufacturing (also known as 3D printing), a group of techniques that produce scaffolds by adding materials usually layer-by-layer, which offer significant advantages for the fabrication of these novel scaffolds (e.g., low cost, high accuracy and high repeatability) for both primary bone cancer and metastatic bone cancer applications.

Scaffolds with advanced functional materials

Recently, researchers developed 3D-printed scaffolds incorporating different functional materials (instead of conventional chemotherapeutics or anticancer drugs). Hou et al. [119, 120] proposed the concept of dual-functional scaffolds (Figs. 2a and 2b) for bone cancer treatment and subsequent bone regeneration using graphene and graphene oxide (GO) fillers (up to 9 wt%). The first function (treatment) aims to induce cancer cell death, while the second function (regeneration) targets the induction of new bone formation. The poly(ε-caprolactone) (PCL)/graphene and PCL/GO scaffolds were produced using a screw-assisted extrusion-based additive manufacturing system. The results of in vitro cell experiments conducted with human adipose-derived stem cells (hADSCs) and sarcoma osteogenic (Saos-2) cells showed that low concentrations of graphene could slightly promote the viability of hADSCs, while high concentrations could inhibit the viability of both hADSCs and Saos-2 cells (Figs. 2c and 2d). The findings also revealed that PCL scaffolds containing high concentrations of graphene exhibit a stronger inhibition effect on Saos-2 cells than on hADSCs. It was also observed that low concentrations of GO inhibit the viability of hADSCs (Fig. 2c). It also seemed that GO had greater inhibition ability on cell viability than graphene. The

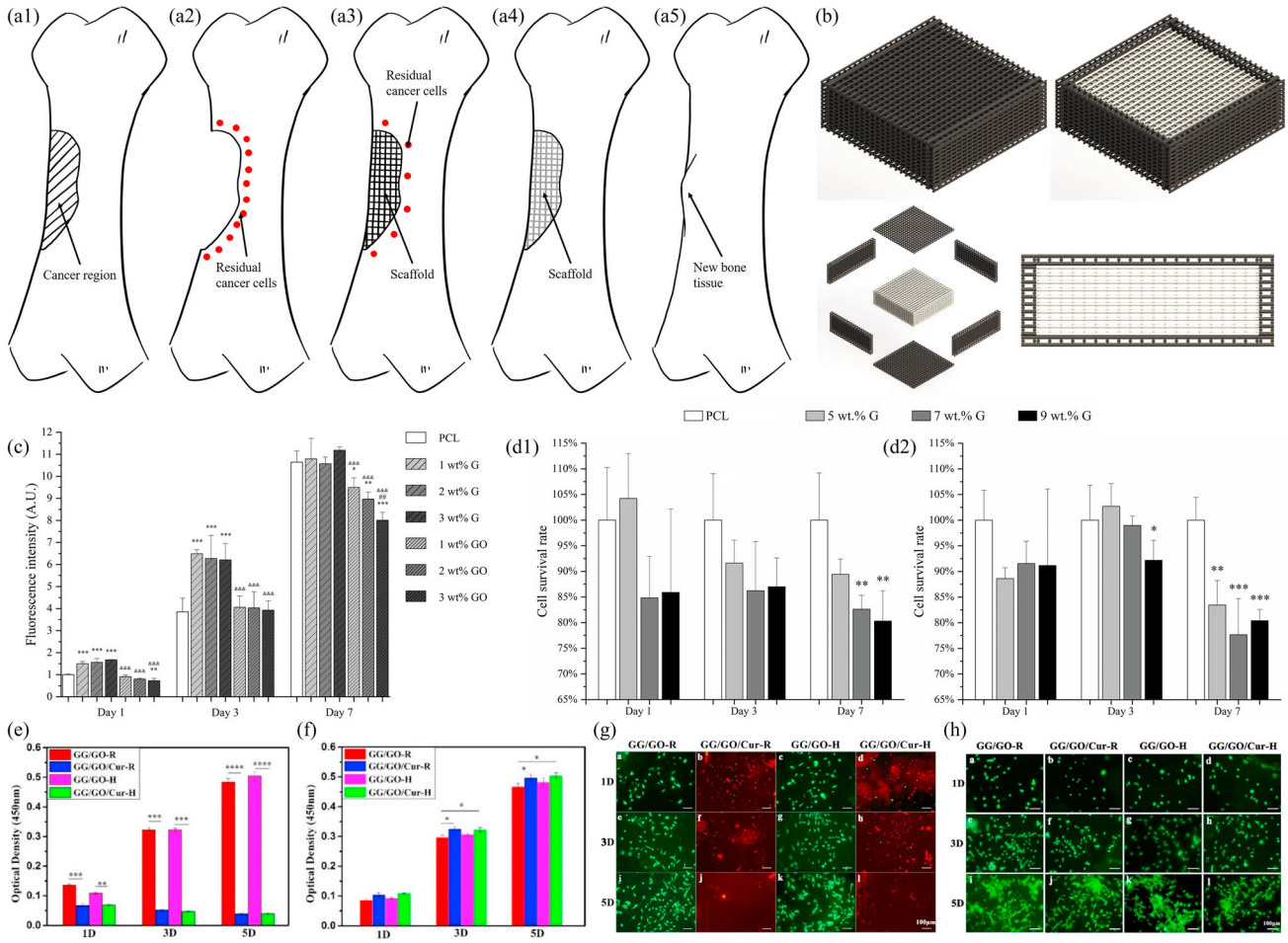

Fig. 2 **a1**–**a5** Dual-functional scaffolds for bone cancer applications. **a1** Bone with a cancer region is detected. **a2** Bone with possible residual cancer cells (red) after tumor resection. **a3** Treatment effect of the implanted dual-functional scaffold: the initial layers of scaffold containing a cytotoxic material will induce the death of possible remaining cancer cells in the surrounding tissue. **a4** Regeneration phase of the implanted dual-functional scaffold: after a certain period, the layers responsible for the treatment phase disappeared (degradation mechanism), and the layers of biocompatible materials will start recruiting healthy cells promoting cell attachment, proliferation, and differentiation, inducing new bone formation. **a5** Bone with regenerated tissue. **b** Different views of the dual-functional scaffolds, where the outer layers (black) are responsible for the treatment function and the inner layers (white) are responsible for the regeneration function. **c** Viability of hADSCs after 1, 3, and 7 days of cell seeding on PCL scaffolds, 1 wt% G scaffolds, 2 wt% G scaffolds, 3 wt% G scaffolds, 1 wt% GO scaffolds, 2 wt% GO scaffolds, and 3 wt% GO scaffolds. The percentage of surviving (**d1**) hADSCs and (**d2**) Saos-2 cells after 1, 3, and 7 days of cell seeding on 5 wt% G scaffolds, 7 wt% G scaffolds, and 9 wt% G scaffolds, with PCL scaffold as the reference (Reproduced from [119], Copyright 2020, with permission from Whioce. Reproduced from [120], Copyright 2020, with permission from Mary Ann Liebert). Viability of **e** MG-63 cells and **f** MC3T3 cells after 1, 3, and 5 days of cell seeding on GG/GO-R scaffolds, GG/GO/Cur-R scaffolds, GG/GO-H scaffolds, and GG/GO/Cur-H scaffolds. R denotes linear lattice, and H denotes honeycomb filling pattern (*P < 0.05, **P < 0.01, ***P < 0.001, ****P < 0.0001). Live/dead confocal microscopy images of **g** MG-63 cells and **h** MC3T3 cells on GG/GO-R scaffolds, GG/GO/Cur-R scaffolds, GG/GO-H scaffolds, and GG/GO/Cur-H scaffolds after 1, 3, and 5 days of cell seeding (Reproduced from [121], Copyright 2021, with permission from Elsevier)

proposed dual-functional scaffolds presented a high potential for bone cancer treatment and recurrence prevention.

Zhu et al. [121] fabricated gellan gum/GO (GG/GO) scaffolds using an extrusion-based 3D printing system equipped with a 22G needle, nozzle temperature of 37 °C, substrate temperature of 25 °C and printing speed of 10 mm/s. Different filling patterns were considered, and the produced scaffolds were soaked in curcumin (Cur) solution to obtain GG/GO/Cur scaffolds. The produced GG/GO/Cur scaffolds could release 30% of the loaded Cur after 14 days in acidic medium (cancer environment). In vitro cell studies were conducted using mouse osteoblast MC3T3 cells and human osteosarcoma MG-63 cells. Based on the CCK-8 assay, the results showed that the fabricated GG/GO/Cur scaffolds could inhibit the viability of MG-63 cells by 50%, 82%, and 93% on day 1, 3, and 5, respectively, which were signifi-

cantly lower compared to the GG/GO scaffolds (Fig. 2e). It was also possible to observe that MC3T3 attachment and proliferation on GG/GO/Cur scaffolds was significantly better than GG/GO scaffolds (Fig. 2f). The results were confirmed by live/dead confocal microscopy images of MG-63 cells and MC3T3 cells on the different scaffolds (Figs. 2g and 2h). No significant differences were observed regarding the different filling patterns.

Besides carbon nanomaterials, other materials like selenium have also been investigated for bone cancer applications. However, due to the relatively complex material preparation and characterization process, a limited number of publications have reported the use of selenium for 3D scaffolds. Most studies focused on the incorporation of selenium into ceramic, polymeric, and metallic nanoparticles, as well as a coating of metallic substrate [122–137]. These studies suggested that selenium is an effective functional material that can be used to treat bone cancer problems without affecting normal cells, also promoting bone regeneration, which is related to its antioxidant and prooxidant properties.

Scaffolds with advanced functional materials have great potential for bone cancer treatment and bone regeneration applications, not requiring additional assistance measures after clinical operation. Moreover, due to the use of biocompatible and biodegradable materials, no second operation is required, which accelerates recovery time. Through the development of novel materials and advanced manufacturing technologies, significant advances are expected in this field.

Drug-loaded scaffolds

Three-dimensional scaffolds have been proposed that are loaded with chemotherapeutics or anticancer drugs such as DOX, and they achieved promising therapeutic results. Chen et al. [138] prepared porous PCL scaffolds (5 mm in height and 10 mm in diameter) using a filament-based extrusion 3D printing machine, loaded the scaffolds by immersing them in a solution containing chitosan, nanoclay, and β-tricalcium phosphate (β-TCP), and freeze-dried the product. PCL was used to provide mechanical strength, while PCL/chitosan/nanoclay/β-TCP/DOX was applied for local sustained drug delivery and bone regeneration. Immortalized human bone marrow-derived mesenchymal stem cells (hBMSCs) were used for in vitro biological evaluation. The scanning electron microscopy (SEM) imaging, confocal microscopy imaging, and DNA quantification results showed that the produced scaffolds were able to support cell attachment, enabling high cell viability and good cell infiltration of hBMSCs. The osteoinductivity of the scaffolds was evaluated through alkaline phosphatase (ALP) and osteocalcin staining, and the results showed that cell mineralization started at day 7 after cell seeding. Moreover, the results of drug release kinetics based on DOX showed a fast release on scaffolds without nanoclay (94% of DOX was released within 4 days) compared to the scaffolds containing nanoclay (up to 47% of DOX was released after 56 days). Moreover, the release profile could be controlled by adjusting the amount of chitosan. The biological impact of the DOX release was not investigated by the authors, but as DOX is an anticancer drug, the results seemed to indicate a significant potential of these scaffolds for both cancer treatment and bone regeneration. This was confirmed by Ahangar et al. [22] using polymeric scaffolds loaded with DOX. These scaffolds were produced using a Flashforge Creator Pro 3D printing system (Flashforge, China) with PORO-LAY filaments (Lay-FOMM 40/60 and Gel Lay; Kai Parthy, Germany), including a nozzle diameter of 0.3 mm, printing temperature of 220 °C, bed temperature of 50 °C, and printing speed of 18 mm/s. DOX was loaded onto the scaffolds in a laminar flow safety cabinet. The produced scaffolds were evaluated in terms of morphology, drug-release kinetics, and biological performance. The results showed that 60–75% of the loaded DOX was released from the scaffolds after 7 days (Figs. 3a and 3b). Prostate cancer LAPC4 cells and patient-derived prostate cancer spine metastases cells were used for the in vitro biological evaluation. Both the Alamar blue and MTT assay results showed that the metabolic activity of LAPC4 cells was reduced after 7 days of treatment, and the Gel Lay scaffolds exhibited the lowest metabolic activity (Figs. 3c and 3d). In the case of patient-derived prostate cancer spine metastatic cells, the decrease in metabolism was more significant, which might be due to the increased sensitivity of these cells to DOX. Overall, the produced DOX-loaded scaffolds significantly reduced metabolic activity, proliferation, migration, and spheroid growth of both the LAPC4 cells and the patient-derived prostate cancer spine metastases cells.

Lahr et al. [139] produced medical-grade PCL scaffolds using the melt-electrospinning technique and loaded the scaffolds with DOX by soaking them in a DOX solution. The in vitro drug release profiles showed that 72%, 80%, and 88% of the loaded DOX was released after two days from the scaffolds containing 0.4, 2, and 10 μg/mg DOX, respectively. In addition, the in vitro viability of Saos-2 cells decreased to $(80 \pm 7)\%$, $(54 \pm 6)\%$, and $(27 \pm 5)\%$ after 2 days of treatment with the scaffolds containing 0.4, 2, and 10 μg/mg, respectively, and further decreased to $(68 \pm 3)\%$, $(4 \pm 2)\%$, and $(1.2 \pm 0.1)\%$ after 5 days, respectively. In vivo biological studies were conducted using female NOD-SCID IL2Rγnull (NSG) mice xenografted with Saos-2 cells. Scaffolds loaded with 1%, 5%, and 10% of the administered intravenous dose of DOX (4 mg/kg body weight) were evaluated and compared with the direct intravenous administration group without using scaffolds. The results showed that the 10% scaffold group exhibited a significant decrease of cancer cell invasion and the increase in cancer cell death in comparison with the

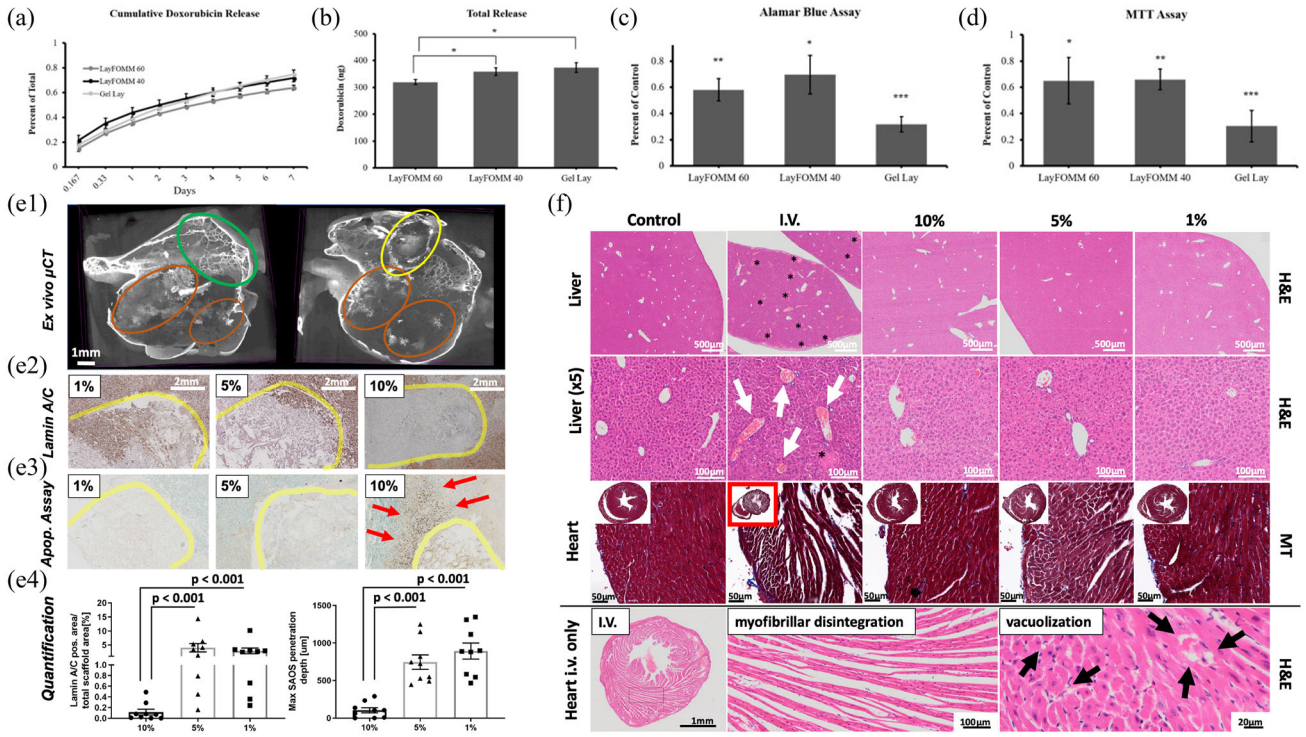

Fig. 3 **a** Release curve of LayFoMM 60 discs, LayFoMM 40 discs, and GelLay discs loaded with DOX over 7 days. **b** Total amount of DOX released from LayFoMM 60 discs, LayFoMM 40 discs, and GelLay discs. Metabolic activity of LAPC4 cells treated with DOX-loaded LayFoMM 60 discs, LayFoMM 40 discs, and GelLay discs for 7 days, assessed through **c** Alamar blue assay and **d** MTT assay. $^{*}P < 0.05$, $^{**}P < 0.01$, and $^{***}P < 0.001$ (Reproduced from [22], Copyright 2018, with permission from MDPI). **e1** Ex vivo micro-CT reconstruction of the orthotopic niche in two different planes, showing the trabecular network (green), ramiform calcifications (brown), and the defect zone (yellow) containing the scaffolds loaded with DOX. **e2** Lamin A/C staining at the region of the scaffolds loaded with DOX (yellow), showing the local invasion pattern of Saos-2 cells (brown) into the scaffolds loaded with 1%, 5%, and 10% of the administered intravenous DOX dose (4 mg/kg body weight). **e3** Apoptotic assay results showing the induction of apoptosis (red) in mice treated with scaffolds loaded with 1%, 5%, and 10% of the administered intravenous DOX dose (4 mg/kg body weight). **e4** Quantitative infiltration area and penetration depth analysis of Saos-2 cells in mice treated with scaffolds loaded with 1%, 5%, and 10% of the administered intravenous DOX dose (4 mg/kg body weight). **f** Hematoxylin–eosin (H&E) staining of the liver (the white arrows show central vein congestion and the black asterisks show multiple necrotic foci). Masson's trichrome and H&E staining of heart cross-sections through both ventriculi (the red box shows right ventricular dilation, the black arrows show vacuolization of cardiomyocytes) in mice treated with scaffolds loaded with 1%, 5%, and 10% of the administered intravenous DOX dose (4 mg/kg body weight) (Reproduced from [139], Copyright 2020, with permission from Elsevier)

1% and 5% groups (Fig. 3e). After 14 days of treatment, in contrast to the scaffold approach, the direct intravenous DOX administration presented side effects as observed by a significant body and organ weight reduction (Fig. 3f).

In addition to DOX, other chemotherapeutics such as 5-FU, ifosfamide, methotrexate, and cisplatin have been evaluated for bone cancer cells. Salmoria et al. [140] investigated polythene (PE)/5-FU waffles manufactured using laser-based powder bed fusion with different laser power densities. In this process, PE was mixed with 5-FU in a rotator for 10 min at 30 r/min and sintered with a CO_2 laser (9 W). The waffles were produced using a laser beam diameter of 250 µm, powder bed temperature of 45 °C, laser scanning speed of 350 mm/s, layer thickness of 250 µm, hatch space of 125 µm, and laser power ranging between 3 and 5 W. The results showed that the waffles produced using 3 W presented lower flexural modulus than those using 5 W due to a lower degree of sintering, and the PE/5-FU waffles presented lower flexural modulus than PE waffles. Similar results were observed for the fatigue strength. The drug release results showed an initial burst release of the loaded drug (50 mg/g) in the first 4 h, and a slower and constant rate in the following 2 days. The waffles produced using 3 W exhibited a faster drug release due to high porosity. Salmoria et al. [141] also fabricated implantable PCL/5-FU tablets using laser-based powder bed fusion with different values of laser power (3 and 7 W). The produced PCL/5-FU tablets also exhibited an initially rapid drug release and then a long-term slow release. More recently, the authors produced PE/5-FU intrauterine devices loaded with progesterone for ovarian cancer applications [142].

Wang et al. [143] fabricated poly-L-lactic acid (PLLA) cylindrical and spherical implants using a vat photopolymer-

ization system. The produced PLLA implants were soaked in dichloromethane solution containing DOX, ifosfamide, methotrexate, and cisplatin. The results showed that the spherical implants had higher drug loading efficiency than the cylindrical ones, suggesting that the shape of the implant affects the drug encapsulation efficiency. In vivo studies were also conducted using nude mice xenografted with human osteosarcoma U_2OS cells. The drug-loaded PLLA implants were implanted after tumor resection and the treatment effect was compared with the intraperitoneal drug injection group. The implanted drug-loaded implants could sustain the release of methotrexate, DOX, ifosfamide, and cisplatin for up to 12 weeks, and no tumor recurrences were observed.

Very few studies have reported on the use of drug-loaded scaffolds to treat bone cancer. However, a number of papers focused on different cancer types presenting high metastasis risk to bone tissue, and thus they are considered relevant within the scope of this review. Yi et al. [144] investigated the use of 3D-printed poly(lactide-co-glycolide)/PCL/5-FU (PLGA/PCL/5-FU) patches as anticancer drug delivery systems (Figs. 4a and 4b). Different concentrations of 5-FU (1, 5, 10, and 15 wt%, named as P10, P50, P100, and P150) were incorporated into PCL/PLGA blends (at a ratio of 1:1) and processed using an extrusion-based multi-head deposition system under a pressure of 600 kPa and a temperature of 140 °C. The patches were produced using different layers (2, 4, and 8) and fiber deposition layouts (latticed, slant, and triangular pattern), allowing for different drug release rates due to differences in the surface area. The results showed that both slanted and triangular patches presented slower 5-FU release rates than the lattice patches. Moreover, it was possible to observe that the patches with the highest 5-FU concentration (15 wt%) released 30% of the loaded drug after 4 weeks. The in vitro biological experiment showed that all produced patches reduced the proliferation of human pancreatic cancer MIA PaCa-2 cells to less than 50%, while maintaining that of hADSCs over 50%, indicating that the produced patches were more effective on cancer cells than healthy cells. The results of in vivo tests conducted on male Balb/c nude mice xenografted with MIA PaCa-2 cells suggested that the 10 wt% patches presented a better inhibition effect on cancer cells and less toxicity on healthy cells. Additionally, no mouse died during the experiment, indicating the low systemic toxicity on internal organs. These results seemed to prove that the 3D-printed drug-loaded patches facilitate local drug delivery with limited side effects. Yang et al. [145] produced PLGA scaffolds containing 5-FU and NVP-BEZ235 (PFN scaffolds) using a near-field electrospinning approach with a flow rate of 0.16 mL/h, 2.8 kV voltage and 3 mm distance between the printing needle and the collector. The scaffolds presented different average pore sizes (50, 100, 150, and 200 μm) and drug loads (6% of 5-FU and 0.005% of NVP). The drug release kinetics results showed that both 5-FU and NVP had a fast release in the first 7 days. It was also observed that the release rate increases by enlarging the pore size. In vitro biological studies were conducted using the MTT assay with human breast cancer MDA-MB-231 cells and NIH 3T3 fibroblasts. The anti-tumor activity of the PFN scaffolds was compared with free drugs (5-FU, NVP), dual drugs (5-FU + NVP), and control groups. After 4 days of treatment, the dual drug group exhibited lower cell viability than the other groups. After 7 days, the PFN scaffolds inhibited 37.83% of MDA-MB-231 cells, which was higher than the control (2.37%), 5-FU (15.19%), NVP (7.66%), and dual drug (21.47%) groups. The results also showed that the PFN scaffolds did not affect the NIH 3T3 fibroblasts' cell growth. These findings were confirmed by both confocal microscopy and Annexin V-PE/7-AAD cell apoptosis assay. The in vivo anticancer properties of PFN scaffolds were evaluated on MDA-MB-231-bearing mice. After 4 weeks of therapy, the tumor volumes were significantly smaller ($< 600\ mm^3$) in the case of PFN scaffolds than the tumor volumes in the dual drug ($900\ mm^3$), control, and single drug groups (both around $1400\ mm^3$) (Figs. 4c–4g). The H&E staining imaging results suggested that the PFN scaffolds caused necrosis within the tumor tissues and reduced metastases in the lungs, while metastases were detected in the other groups. All of the results seemed to suggest that PFN scaffolds correspond to a viable approach to treat tumors with negligible side effects on other organs. Chou et al. [146] used an extrusion-based 3D printer (Hyrel system 30 M) to produce nanogel discs containing PTX and rapamycin. Briefly, solgels were prepared by mixing poloxamer, PTX, rapamycin, and tert-butanol, and were printed at a printing speed of 10 mm/s. Finally, the printed discs were dehydrated in an oven at 37 °C for 24 h. The drug release results showed that the discs presented slower release profiles than sol-gels and that the release of PTX was also slower than rapamycin. The relevant in vivo studies were based on female athymic NCr-nu/nu mice xenografted with ES-2-luc cells, and the results showed that the drug-loaded discs could successfully deliver the drugs peritoneally, reducing both the risk of post-surgical peritoneal adhesion and the progression of tumor, thus increasing the survival rate. Dang et al. [147] used an extrusion-based additive manufacturing system to produce PCL scaffolds (diameter of 6 mm and height of 0.75 mm) and loaded with DOX. Female NOD-SCID IL2Rγnull (NSG) mice xenografted with MDA-MB-231 cells were used for their in vivo studies (Fig. 4h), and the results showed that the DOX-loaded PCL scaffolds delayed the growth and recurrence of cancer (Figs. 4i and 4j). The produced scaffolds also reduced the cancer metastases in the lungs, liver, and spleen.

Metal structures have also been investigated as local drug delivery systems. Aiming to develop bone implants with improved biointegration and anticancer properties, Maher

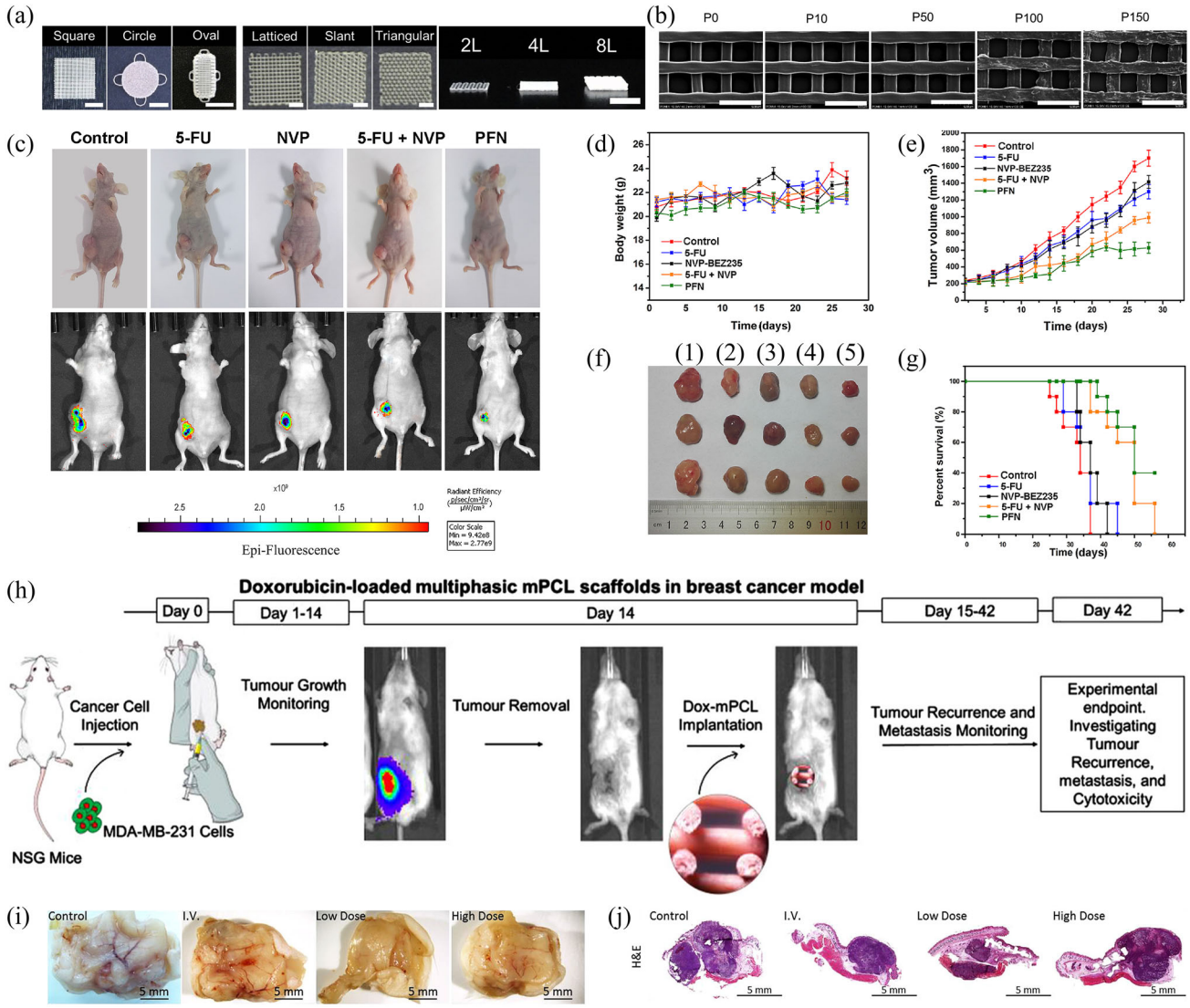

Fig. 4 **a** Patches with various shapes (square, circle, and oval, scale bar = 5 mm), pores (latticed, slant, and triangular, scale bar = 2 mm), and layers (2, 4, and 8, scale bar = 2 mm). **b** SEM images of the surface of P0, P10, P50, P100, and P150 patches. Scale bar = 500 μm (Reproduced from [144], Copyright 2016, with permission from Elsevier). **c** Photographs and in vivo fluorescence images of mice after 4 weeks of treatment in the control group, 5-FU group, NVP group, 5-FU + NVP group, and PFN group. **d** Body weight changes of mice in the control group, 5-FU group, NVP group, 5-FU + NVP group, and PFN group. **e** Tumor volume changes of mice in the control group, 5-FU group, NVP group, 5-FU + NVP group, and PFN group. **f** Photographs of tumors collected from mice under different treatment approaches after 4 weeks of treatment. **f1** Control, **f2** 5-FU, **f3** NVP, **f4** dual drugs (5-FU/NVP), **f5** PFN scaffolds. **g** Survival curves of mice in the control group, 5-FU group, NVP group, 5-FU + NVP group, and PFN group within 60 days (Reproduced from [145], Copyright 2020, with permission from Elsevier). **h** Workflow of in vivo experiments. **i** Bright-field and **j** H&E staining images of the recurrent tumors at the primary tumor site in the control group, I.V. group, low-dose group, and high-dose group (Reproduced from [147], Copyright 2020, with permission from John Wiley and Sons)

et al. [148] used a laser-based powder bed fusion system equipped with 300 W laser (1070 nm) to produce Ti6Al4V wafers under an inert argon atmosphere. The produced wafers were submitted to an anodization process to create a surface topography suitable for bone applications, and they were finally loaded with DOX and apoptosis-inducing ligand (Apo2L/TRAIL) under vacuum. The in vitro results showed that, after 24 h of treatment, the anticancer drug-loaded wafers were able to significantly reduce the viability of MDA-MB-231-TXSA cells, indicating that it can be a viable approach to treat bone cancers.

Drug-loaded scaffolds have shown good bone cancer treatment efficacy with very limited side effects due to the localized drug delivery mechanism. For this approach, how-

ever, the sustained and controllable release of drugs is critical. The existing studies have been limited to qualitative research, hence more comprehensive investigations on precise drug-release rates are needed.

Scaffolds for photothermal/magnetothermal therapy

As cancer cells are temperature sensitive, the use of scaffolds containing photo-sensitizers or magneto-sensitizers seems to represent a feasible alternative to treat bone cancers. These scaffolds generate heat when irradiated with NIR or exposed to a magnetic field. Zhang et al. [149] used pressure-assisted extrusion-based 3D printing systems to produce PCL and mesoporous bioactive glass (MBG, Si/Ca/P molar ratio of 80/15/5) composite scaffolds containing different concentrations of Fe_3O_4 (0, 5, 10, and 15 wt%) (Figs. 5a and 5b). Briefly, MBG powders and magnetic Fe_3O_4 nanoparticles were mixed and added into a PCL solution (the weight ratio between Fe_3O_4/MBG and PCL was 62:38), forming a paste that was then 3D-printed (nozzle diameter of 0.25 mm, pressure ranged between 1.5–3.0 bar, and printing speed ranged between 1.5 and 5 mm/s), producing scaffolds with uniform macropores (400 μm), high porosity (60%), and compressive strength varying between 13–16 MPa. Under an alternative magnetic field (strength of 180 G and frequency of 409 kHz), the temperature of the 15 wt% Fe_3O_4/MBG/PCL scaffolds rapidly increased from 20 to 43 °C within 2 min. The results also showed that the rate of temperature increase rises by elevating the Fe_3O_4 concentration. Moreover, the scaffolds were loaded with DOX, and drug release studies showed that around 30% of the loaded DOX was released on the first day. Despite the potential of these scaffolds for cancer applications, the authors did not perform any biological studies to evaluate the concept. Their biological studies were limited to in vitro proliferation and differentiation assays using primary hBMSCs without applying any magnetic field. The results showed that the addition of magnetic Fe_3O_4 nanoparticles could promote cell proliferation, ALP activity, osteogenesis-related gene expression (RUNX2, OCN, BSP, BMP-2, and Col-1), and ECM mineralization without influencing the apatite mineralization ability.

Dong et al. [150] fabricated akermanite (AKT) scaffolds loaded with different concentrations of Fe_3O_4 (0, 0.1, 0.5, 1.0, and 1.5 M) and CaO_2 (2.5 μg/μL) using an extrusion additive manufacturing system. The AKT-Fe_3O_4-CaO_2 scaffolds were able to reach 28, 40, 53, 75, and 90 °C (for 0, 0.1, 0.5, 1.0, and 1.5 M Fe_3O_4, respectively) under an alternative magnetic field (frequency of 500 kHz, output current of 22 A, and coil diameter of 10 cm). The in vitro studies showed that the viability of human osteosarcoma MNNG/HOS cells seeded on the scaffolds (without magnetic field) was significantly reduced in pH 6.0 and slightly reduced in pH 7.4 after one day of cell seeding. Similar trends were observed in the case of AKT-Fe_3O_4-CaO_2 scaffolds under the alternative magnetic field for 1 min. Furthermore, the AKT-Fe_3O_4-CaO_2 scaffolds (without a magnetic field) seeded with bone marrow stromal cells sustained cell spreading and promoted osteogenesis as observed by gene expression (BMP2, OCN, RUNX2, and COL1) and ALP activity. In vivo studies were conducted on female Balb/c nude mice xenografted with MNNG/HOS cells. The inhibition efficacy of AKT-Fe_3O_4 and AKT-Fe_3O_4-CaO_2 scaffolds under magnetic field (every 2 days) were 15.8% and 45.3%, significantly lower than the values (63.2% and 91.4%) observed for AKT-Fe_3O_4 and AKT-Fe_3O_4-CaO_2 scaffolds without applying the magnetic field (Figs. 5c–5f). Moreover, no significant pathological toxicity was observed in the major organs (heart, lung, spleen, liver, and kidney) in any of the groups. The inhibition effect was attributed to the Fenton-like effect, a reaction between Fe_3O_4 and CaO_2 generating OH and increasing the reactive oxygen species (ROS) level, which induces the termination of cancer. Moreover, micro-CT and CLSM images showed good in vivo osteogenesis capability of AKT-Fe_3O_4-CaO_2 scaffolds based on a male Sprague-Dawley rat model.

Wang et al. [151] combined additive manufacturing with a hydrothermal method for the in situ growth of molybdenum disulfide (MoS_2) nanosheets on the strut surface of AKT scaffolds (MS-AKT scaffolds). Under NIR irradiation (0.5 W/cm^2), it was possible to observe that the MS-AKT scaffolds could rapidly reach 115 °C after 5 min of irradiation under a dry environment (air), and 50 °C after 10 min under wet conditions (phosphate-buffered saline). In vitro cell studies were conducted using Saos-2, MDA-MB-231 cells, and rabbit BMSCs, and the results showed that, after submitting the MS-AKT scaffolds to a cycle of three irradiation stages (0.6 W/cm^2, 10 min), the viability of MDA-MB-231 cells was reduced to around 5%. Saos-2 cells were also inhibited. Without the irradiation, MS-AKT scaffolds were able to promote rabbit BMSCs proliferation and upregulate the expression of osteogenic genes (Runx2, OCN, OPN and ALP). The in vivo biological studies were based on Balb/c mice xenografted with Saos-2 cells (Figs. 5g–5i). In the case of combining MS-AKT scaffolds with irradiation (0.5 W/cm^2, 10 min, every 2 days) almost no tumors were observed after 14 days, a value significantly lower when compared to the other considered cases (Fig. 5j). Zhuang et al. [152] prepared ceramic inks containing AKT and Fe (Figs. 5k–5m) to produce 3D-printed scaffolds using an extrusion-based system. The authors conducted in vitro studies using murine osteosarcoma LM-8 cells and considered three conditions: magnetic field (896.8 A/m) only; NIR (0.70 W/cm^2) only and a combination of magnetic field and NIR. The findings revealed that cell viability decreased to 59.2% in the case of magnetic field, to 81.6% in the case of NIR, and to 2.0% in the combined case. The

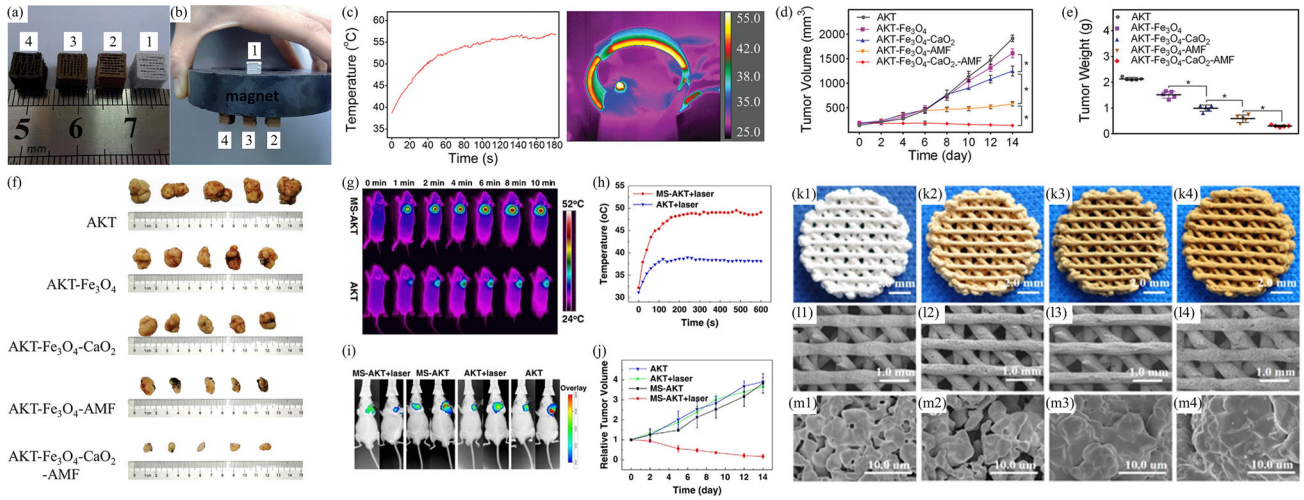

Fig. 5 **a** Photograph of (1) MBG/PCL, (2) 5Fe_3O_4/MBG/PCL, (3) 10Fe_3O_4/MBG/PCL, and (4) 15Fe_3O_4/MBG/PCL scaffolds. **b** Fe_3O_4/MBG/PCL scaffolds attracted to a magnet (Reproduced from [149], Copyright 2014, with permission from Royal Society of Chemistry). **c** Magnetic-heating curve and infrared bitmap of the AKT-Fe_3O_4-CaO_2 scaffold implanted in the tumor after exposure to the magnetic field. **d** Time-dependent tumor volume curves of MNNG/HOS-bearing mice treated with AKT scaffolds, AKT-Fe_3O_4 scaffolds with and without irradiation, and AKT-Fe_3O_4-CaO_2 scaffolds with and without irradiation. **e** The weight of excised tumor from MNNG/HOS-bearing mice treated with AKT scaffolds, AKT-Fe_3O_4 scaffolds with and without irradiation, and AKT-Fe_3O_4-CaO_2 scaffolds with and without irradiation after 14 days of treatment. $^*P < 0.05$. **f** Photographs of excised tumors after treatment using AKT scaffolds, AKT-Fe_3O_4 scaffolds with and without irradiation, and AKT-Fe_3O_4-CaO_2 scaffolds with and without irradiation (Reproduced from [150], Copyright 2019, with permission from John Wiley and Sons). **g** Thermal images and **h** temperature changes of tumor-bearing mice after being implanted with MS-AKT and AKT scaffolds under NIR irradiation for up to 10 min. **i** Whole-body fluorescence imaging of mice after 0 day (left) and 7 days (right) of treatment with MS-AKT scaffolds with and without irradiation, and with AKT scaffolds with and without irradiation. **j** Relative tumor volume of mice treated with MS-AKT scaffolds with irradiation, MS-AKT scaffolds without irradiation, AKT scaffolds with irradiation, and AKT scaffolds without irradiation (Reproduced from [151], Copyright 2017, with permission from Springer Nature). **k** Photographs and (**l** and **m**) SEM images of (**k1**, **l1**, and **m1**) AKT scaffolds, (**k2**, **l2**, and **m2**) 1Fe-AKT scaffolds, (**k3**, **l3**, and **m3**) 2Fe-AKT scaffolds, and (**k4**, **l4**, and **m4**) 3Fe-AKT scaffolds (Reproduced from [152], Copyright 2019, with permission from American Chemical Society)

Fe-AKT scaffolds also showed good cell adhesion, proliferation, and osteogenic properties (high expression levels of RUNX2, OPN, OCN, and BMP2 genes) on rabbit BMSCs.

Further materials such as bioglass (BG) have also been used to fabricate photothermal/magnetothermal scaffolds. Yang et al. [153] prepared BG scaffolds using a pressure-assisted extrusion system, which were then soaked in a solution containing mesoporous silica-coated 2D Nb_2C MXene and S-nitrosothiol to produce MS/MXene-BG-SNO scaffolds (shortly referred to as MBS scaffolds). Once irradiated under NIR (1064 nm, 1.0 W/cm^2) for 10 min, the temperature rapidly increased to 52 °C. A correlation between temperature increase and light intensity was also established. In vitro studies were conducted using Saos-2 cells, and the results showed that after irradiation for 10 min (1.0 W/cm^2), the viability of Saos-2 cells decreased to 25–35% and further decreased to 20–30% by increasing the irradiation time to 30 min. In vivo cell studies were conducted using female Balb/c nude mice xenografted with Saos-2 cells. In this case, MBS scaffolds were compared to BG scaffolds loaded with Nb_2C (NBGS) considering stages of irradiation for 10 min and NIR intensity of 1.0 W/cm^2 every 2 days. The results showed that both NBGS and MBS eliminated cancer without recurrence after 2 weeks of treatment due to the precise control of nitric oxide release and the anticancer effects of nitric oxide. Moreover, the MBS group eliminated cancer faster than the NBGS group, as observed from the staining results showing more apoptotic cells. No significant body weight change and metastasis were observed in other major organs (heart, liver, spleen, lung, and kidney). Moreover, the in vivo studies involving on male Sprague–Dawley rats showed that the MBS scaffolds exhibited good osteogenic and angiogenic properties. Similar results were obtained by Pan et al. [154] using BG scaffolds loaded with Ti_3C_2 on female Balb/c nude mice xenografted with Saos-2 cells (Fig. 6a) and Sprague–Dawley (SD) rats. The in vitro results revealed good cancer treatment effects and demonstrated that the fabricated scaffolds can support the proliferation and differentiation of human marrow-derived BMSCs, exhibiting enhanced osteogenic capability. The in vivo results also confirmed the output of in vitro cancer treatment. Additionally, the osteogenesis rate of the Ti_3C_2-loaded scaffold was 2.5 times higher than that of BG scaffolds. Wang et al. [155] used BG scaffolds coated with molybdenum disulfide

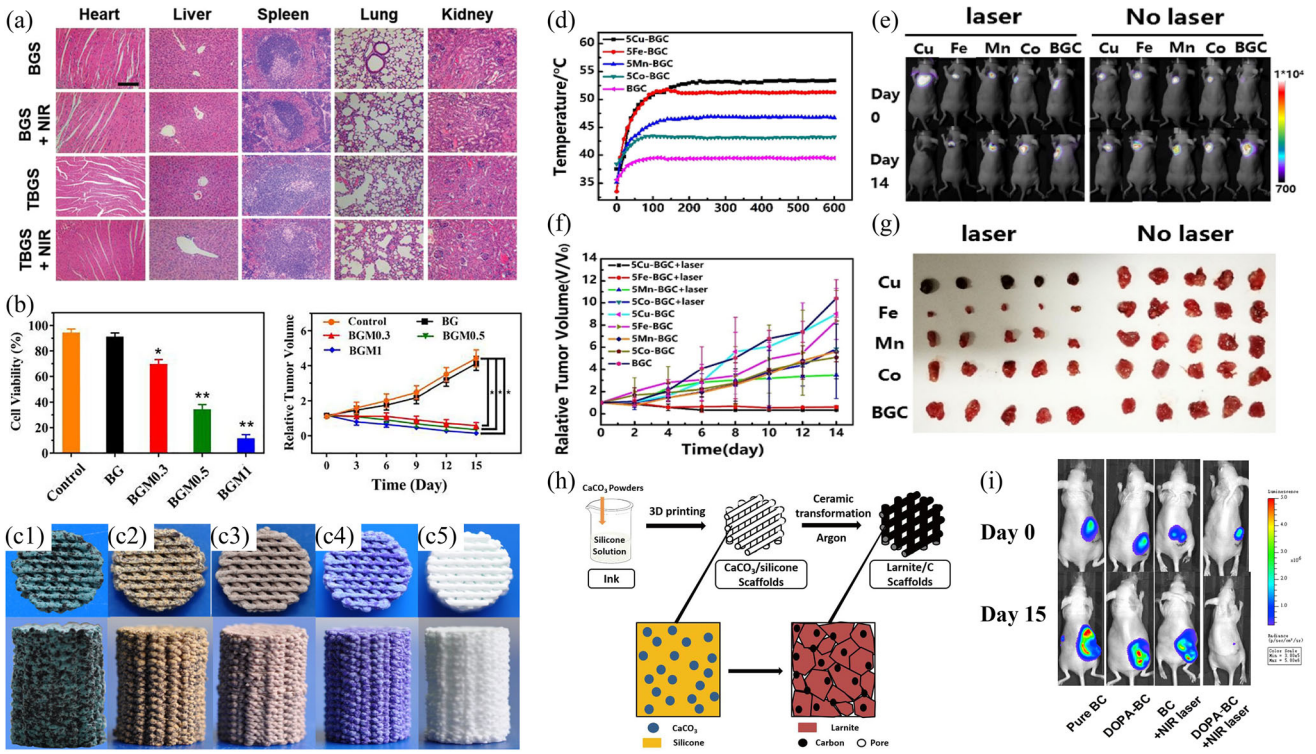

Fig. 6 **a** H&E staining of the major organs of Saos-2-bearing mice on day 14 with BGS scaffolds with and without irradiation, and with TBGS scaffolds with and without irradiation. Scale bars = 100 μm (Reproduced from [154], Copyright 2019, with permission from John Wiley and Sons). **b** Relative cell viability and tumor volume in the control, BG scaffolds with irradiation, BGM0.3 scaffolds with irradiation, BGM0.5 scaffolds with irradiation, and BGM1 scaffolds with irradiation at day 14 (Reproduced from [155], Copyright 2020, with permission from Elsevier). **c1–c5** Photographs of **c1** 5Cu-BGC, **c2** 5Fe-BGC, **c3** 5Mn-BGC, **c4** 5Co-BGC, and **c5** BGC scaffolds. **d** Temperature changes of 5Cu-BGC, 5Fe-BGC, 5Mn-BGC, 5Co-BGC, and BGC scaffolds under irradiation. **e** Whole-body fluorescence images of tumor in mice treated with 5Cu-BGC scaffolds with irradiation, 5Fe-BGC scaffolds with irradiation, 5Mn-BGC scaffolds with irradiation, 5Co-BGC scaffolds with irradiation, and BGC scaffolds with irradiation at day 0 and day 14. **f** Tumor volume changes of mice with 5Cu-BGC scaffolds with and without irradiation, 5Fe-BGC scaffolds with and without irradiation, 5Mn-BGC scaffolds with and without irradiation, 5Co-BGC scaffolds with and without irradiation, and BGC scaffolds without irradiation. **g** Photographs of tumors obtained from different mice treated with 5Cu-BGC, 5Fe-BGC, 5Mn-BGC, 5Co-BGC, and BGC scaffolds with irradiation on day 14 (Reproduced from [158], Copyright 2018, with permission from Elsevier). **h** Schematic illustration of the fabrication process and functions of larnite/C scaffolds (Reproduced from [160], Copyright 2020, with permission from Elsevier). **i** Whole-body bioluminescent imaging of tumor in mice treated with BC scaffolds with and without irradiation, and DOPA-BC scaffolds with and without irradiation (Reproduced from [161], Copyright 2016, with permission from Elsevier)

(MoS_2) on nude rats xenografted with MNNG/HOS cells (Fig. 6b) and SD rats. The in vitro results showed that the produced scaffolds coated with MoS_2 presented a good ability for both cancer treatment and rabbit BMSCs mineralization. The in vivo biological studies confirmed these results in terms of both tumor inhibition and bone regeneration. Dang et al. [156] used BG scaffolds functionalized by $CuFeSe_2$ nanocrystals and prepared by 3D printing and solvothermal synthesis on nude mice xenografted with Saos-2 cells and a New Zealand white rabbit model. Like in previously reviewed cases, both the in vitro and in vivo results confirmed good cancer treatment and bone tissue regeneration ability. Similar findings were obtained using 3D-printed BG scaffolds loaded with DOX on female nude mice xenografted with K7M2wt cells [157].

The effect of the element composition was investigated by Liu et al. [158], wherein a commercially available BG ($CaSiO_3$) was modified by incorporating different levels of Cu, Fe, Mn, and Co ($Cu(NO_3)_2{\cdot}4H_2O$, $Fe(NO_3)_3{\cdot}9H_2O$, $Mn(NO_3)_2{\cdot}4H_2O$ and $Co(NO_3)_2{\cdot}6H_2O$) through a sol–gel method using tetraethyl orthosilicate and triethyl phosphate (Fig. 6c). The sol–gel derived powders were sintered at 800 °C for 3 h, mixed with a Pluronic F-127 solution, and printed using an extrusion-based system. The scaffolds containing Cu exhibited the fastest degradation rate (21.3% weight loss after 28 days) and the best photothermal performance (wavelength of 808 nm and light intensity of 0.48 W/cm^2). The in vivo anticancer properties of the produced scaffolds were evaluated based on nude mice xenografted with Saos-2 cells. The results showed that the scaffolds containing Cu under

NIR irradiation (0.75 W/cm^2 for 15 min, every 2 days) presented the highest cancer inhibition effect (tumor tissue necrosis rate of 94.9%) compared with all other groups (Figs. 6d–6g). Moreover, scaffolds containing Fe and Mn promoted the attachment and proliferation of rabbit BMSCs, scaffolds containing Co had the highest expression level of ALP, and both BG and Cu scaffolds showed the strongest mineralization ability. Similar results were reported by Ma et al. [159], who prepared a mixture of Fe and $CaSiO_3$ powders to produce scaffolds using a laser-based powder bed fusion system under inert conditions. The produced Fe-CaSiO3 scaffolds showed anticancer characteristics both in vitro (under NIR irradiation of 0.6 W/cm^2 for 15 min, every 2 days) and in vivo (under NIR irradiation of 0.8 W /m^2 for 10 min, every 2 days), as well as osteogenesis properties when used without irradiation. Moreover, due to the release of Fe ions during treatment and its interaction with H_2O_2 inside the tumor, ROS generation was induced, enhancing the tumor therapeutic effect of the scaffolds due to the synergistic photothermal and ROS effects.

Fu et al. [160] fabricated porous free carbon-embedding larnite (larnite/C) scaffolds using a pressure-assisted extrusion-based system. Prior to printing, $CaCO_3$ powders were mixed with silicone resin in isopropyl alcohol (Fig. 6h). The printed scaffolds were heated (rate of 2 °C/min for 3 h) in an argon atmosphere up to 1200 °C. Larnite scaffolds, fabricated using sol–gel larnite powders followed by sintering, were used as control for the biological studies. The results showed that the temperature of the larnite/C scaffolds rapidly increased to 61–63 °C (dry conditions) and 46–48 °C (wet conditions) under irradiation (808 nm, 0.75 W/cm^2) for 5 min. The in vitro cell studies therein were conducted using MNNG/HOS cells and rat BMSCs on both larnite and larnite/C-3 scaffolds. The CCK-8 assay results showed that, by increasing the NIR intensity from 0.5 to 1.25 W/cm^2, the viability of MNNG/HOS cells decreased from (70 ± 5)% to (5 ± 2)%. Without irradiation, the larnite/C scaffolds presented better osteogenic results, as confirmed by high rat BMSCs viability and high expression levels of osteogenic markers such as ALP, OCN and Runx-2. The in vivo studies were conducted based on nude mice xenografted with MNNG/HOS cells, and the results showed that the combined use of larnite/C scaffolds and irradiation (0.75 W/cm^2 for 10 min, every 2 days) significantly decreased the tumor volume. In addition, substantial necrosis of the tumor tissue was observed by H&E staining imaging. The reconstructed micro-CT images showed that larnite/C-3 scaffolds resulted in higher bone mineral density (0.41 g/cm^3) and bone volume/tissue volume ratio (40%) compared to larnite scaffolds (0.3 g/cm^3 and 35%).

Dopamine, commonly used to improve the biological performance of scaffolds, has been used to increase the scaffold temperature upon NIR irradiation, thus improving its anticancer capabilities. Ma et al. [161] used an extrusion-based system to produce $Ca_7Si_2P_2O_{16}$ scaffolds. The produced bioceramic scaffolds were soaked in a polydopamine solution and dried to obtain the final polydopamine-bioceramic (DOPA-BC) scaffolds. Upon irradiation with NIR (808 nm, 0.34 W/cm^2), the temperature of DOPA-BC scaffolds increased to 92 °C in a dry environment and to 50 °C in a wet environment. Saos-2 and MDA-MB-231 cells were used to evaluate the in vitro photothermal effect of the DOPA-BC scaffolds. The results showed that under irradiation (0.38 W/cm^2, 10 min), the viability of Saos2 cells and MDA-MB-231 cells decreased to around 99.2% and 97.4%, respectively. In vivo cancer studies were conducted based on female nude mice xenografted with MDA-MB-231 cells both under irradiation (0.38 W/cm^2 for 10 min, every 2 days) and no irradiation. In the case of irradiation, the temperature was observed to rapidly increase to values higher than 50 °C, and the weight of the tumor was significantly reduced (Fig. 6i). In the case of the hyperthermic central area (temperatures above 50 °C), the cancer cells underwent coagulative necrosis caused by cell membrane collapse, protein denaturation, termination of enzyme activity, and mitochondrial dysfunction. In the case of the hyperthermic peripheral region (temperatures above 45 °C), the ablation of tumors was triggered by cancer cell apoptosis. Moreover, histological analysis based on the New Zealand white rabbit model showed that, after 8 weeks of implantation without NIR irradiation, the bone regeneration was stimulated.

Ma et al. [162] investigated the use of GO-modified β-TCP (GO-TCP) scaffolds for bone cancer applications (Figs. 7a and 7b). The TCP powder was mixed with a polyvinyl alcohol (PVA) solution and printed using an extrusion-based machine. Finally, the scaffolds were soaked in a solution containing GO. After NIR irradiation (0.36 W/cm^2) for 10 min, the temperature increased to 71–85 °C at dry conditions and to 39–45 °C at wet conditions, depending on the GO concentration increased from 0.25 to 1 mg/mL. In vitro biological studies were conducted using MG-63 cells and rabbit BMSCs. Under irradiation (0.36 W/cm^2 for 10 min), the GO-TCP scaffolds inhibited 80% of the MG-63 cells, and the cell viability further decreased by 92.6% under a longer irradiation time (30 min). The results also showed that rabbit BMSCs seeded on irradiated GO-TCP scaffolds presented high ALP activity and bone-related gene expression levels (Runx2, OCN, and BSP). In vivo studies were conducted based on nude mice xenografted with Saos-2 cells and the New Zealand white rabbit model considering four different cases: TCP scaffolds with irradiation (0.42 W/cm^2 for 10 min, every 2 days), TCP scaffolds without irradiation, GO-TCP scaffolds with irradiation (0.42 W/cm^2 for 10 min, every 2 days), and GO-TCP scaffolds without irradiation. The findings revealed that the necrosis rate of cancer cells reached up to 83.28% in the GO-TCP scaffolds with NIR irra-

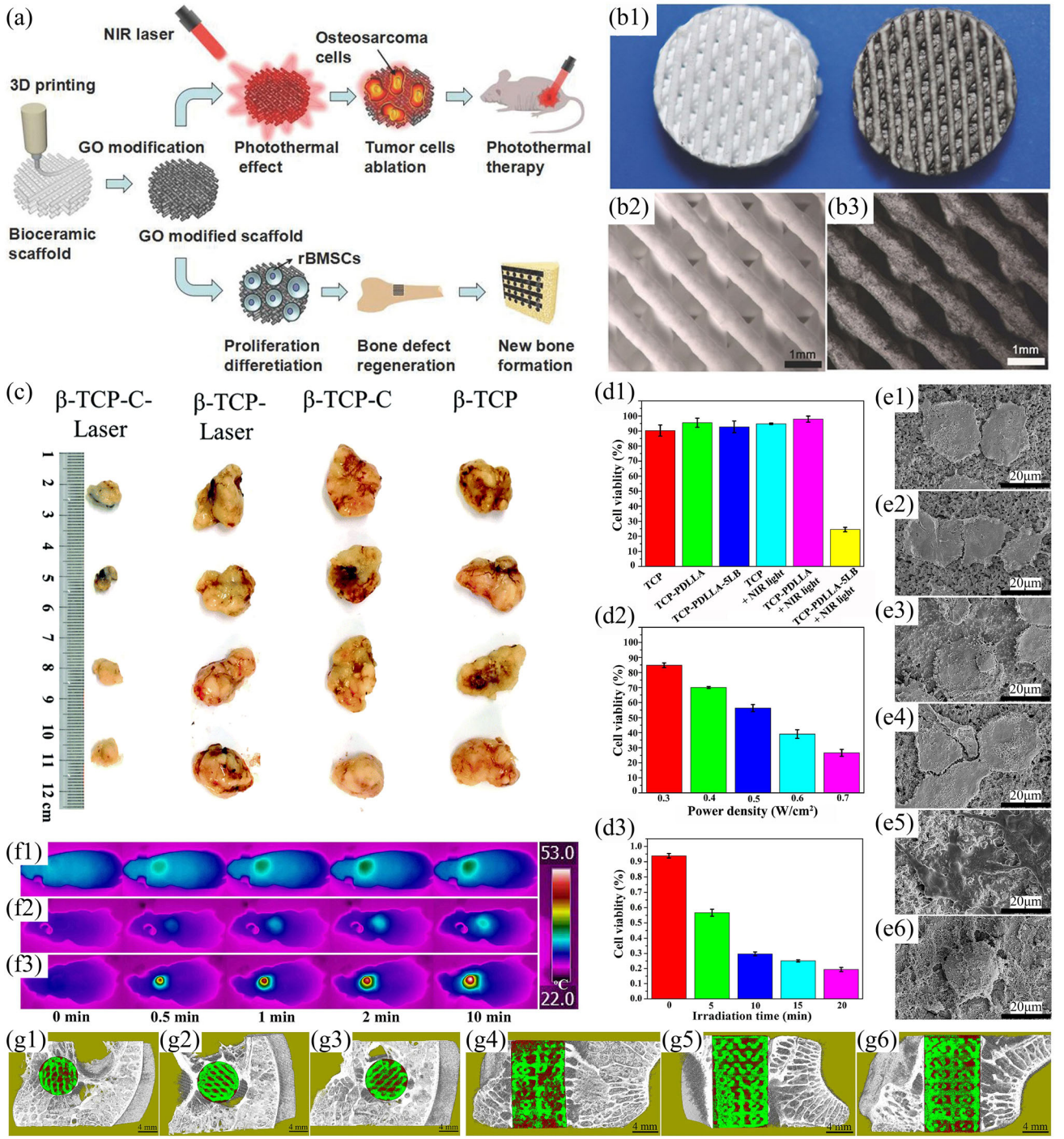

Fig. 7 **a** Schematic illustration of the bifunctional GO-TCP scaffold concept and the in vivo experimental procedure. **b1**–**b3** Photographs of β-TCP (white) and GO-TCP (black) scaffolds (Reproduced from [162], Copyright 2016, with permission from John Wiley and Sons). **c** Photographs of tumors excised after 14 days of treatment using β-TCP scaffolds with and without irradiation, and β-TCP-C scaffolds with and without irradiation (Reproduced from [163], Copyright 2020, with permission from Royal Society of Chemistry). **d1** Viability of Saos-2 cells on TCP scaffolds with and without irradiation, TCP-PDLLA scaffolds with and without irradiation, and TCP-PDLLA-5LB scaffolds with and without irradiation. **d2** TCP-PDLLA-5LB scaffolds irradiated under different NIR light intensities. **d3** TCP-PDLLA-5LB scaffolds irradiated under NIR under different irradiation times. **e1**–**e6** SEM images of Saos-2 cells on TCP (**e1**, **e2**), TCP-PDLLA (**e3**, **e4**), TCP-PDLLA-5LB (**e5**, **e6**) scaffolds without (**e1**, **e3**, **e5**) or with (**e2**, **e4**, **e6**) NIR irradiation. Thermal images of tumor-bearing mice after being implanted with (**f1**) TCP, (**f2**) TCP-PDLLA, and (**f3**) TCP-PDLLA-5LB scaffolds under NIR irradiation. Micro-CT images of TCP (**g1**, **g2**), TCP-PDLLA (**g3**, **g4**), and TCP-PDLLA-5LB (**g5**, **g6**) scaffolds implanted into critical-sized femoral defects of rabbits after 8 weeks (green for scaffolds and red for bone-related tissues) (Reproduced from [164], Copyright 2019, with permission from Elsevier)

diation, which was significantly higher than the other groups. Moreover, the histomorphometric measurements revealed improved osteogenic differentiation of rabbit BMSCs in the GO-TCP scaffolds without irradiation due to the specific bioactive groups (carboxyl and hydroxyl groups) and protein absorbance of GO. Dong et al. [163] studied the use of carbon aerogel (CA)-coated β-TCP (TCP-CA) scaffolds. An ink prepared by mixing TCP powder in a PVA solution was printed using an extrusion-based additive manufacturing system, producing scaffolds that were then coated by immersing the TCP scaffolds in a CA solution. Under NIR irradiation (1.0 W/cm^2) for 10 min, the temperature of the TCP-CA scaffolds increased to 74 °C, while the temperature of the non-coated TCP scaffolds increased to 28 °C. The associated in vitro studies conducted with MNNG/HOS cells under the same irradiation conditions showed that the cell viability significantly decreased in the TCP-CA group in comparison with the TCP group. It was also observed that, without irradiation, the TCP-CA scaffolds enhanced the attachment of bone marrow stromal cells, regulating the subsequent cellular behaviors. The scaffold groups evaluated in the in vitro studies were also considered in the in vivo studies conducted using Balb/c nude mice xenografted with MNNG/HOS cells. The results showed that the use of TCP-CA scaffolds with irradiation (1.0 W/cm^2, keeping 52 °C for 2 min, every 2 days) allowed for a cancer inhibition rate of 81.85%, which was higher than any other cases (Fig. 7c). Moreover, it was observed that TCP-CA scaffolds without irradiation could support in vivo osteogenesis. Dang et al. [164] also used TCP powder in a pluronic F-127 solution to produce scaffolds in an extrusion-based system. Scaffolds were then soaked in a solution containing lanthanum hexaboride (LaB_6) and poly(D,L-Lactic Acid) (PDLLA) at different concentrations (0.01, 0.03, and 0.05 g/mL corresponding to TCP-PDLLA-1LaB_6, TCP-PDLLA-3LaB_6, TCP-PDLLA-5LaB_6, respectively). The results showed that the addition of PDLLA and LaB_6 increased the compressive strength of the scaffolds. Further results showed that, upon irradiating the scaffolds with a NIR laser (808 nm, 0.6 W/cm^2), the temperature of the scaffolds reached 100.7, 119.2, and 128.8 °C under dry conditions (temperatures corresponding to the TCP-PDLLA-1LB, TCP-PDLLA-3LB, TCP-PDLLA-5LB groups, respectively) and 52.3, 62.4, and 66.3 °C, respectively, under wet conditions. Saos-2 cells and rabbit bone marrow stromal cells were used for the in vitro studies and the scaffolds were irradiated under different light intensities (0.3, 0.4, 0.5, 0.6, and 0.7 W/cm^2) for 5, 10, 15, and 20 min. The results showed that cell viability decreased by increasing the NIR intensity and irradiation time (Fig. 7d). For the same NIR intensity and irradiation time, a significant decrease in cell viability was achieved in the TCP-PDLLA-5LB group (Figs. 7d and 7e). The in vitro studies conducted without irradiation demonstrated that the TCP-PDLLA-5LB scaffolds could support the attachment and growth of rabbit bone marrow stromal cells, with higher expression levels of osteogenic-related genes RUNX2, COL 1 and BMP2. In vivo studies were conducted based on nude mice xenografted with Saos-2 cells and a New Zealand white rabbit model (Figs. 7f and 7g). The H&E staining results showed that the NIR-irradiated (0.7 W/cm^2 for 10 min, every day) TCP-PDLLA-5LB scaffolds could inhibit tumor growth, and also support bone-forming activity in vivo, as indicated by micro-CT scanning results (Fig. 7g).

Photothermal/magnetothermal therapy has been widely investigated and subjected to a large number of in vitro and in vivo biological studies [149–164]. Positive results were observed not only in terms of bone cancer treatment but also for bone regeneration. However, these strategies need external assistance such as controllable NIR or magnetic field, which potentially increases the difficulty of the surgical procedure. Moreover, similar to the drug-loaded scaffold approach, these studies focused only on qualitative research. Thus, more comprehensive studies are needed on mathematical models to describe the materials, heat-release, and anticancer effects.

Conclusions and future perspectives

The current clinical approaches for bone cancer include surgery, chemotherapy, radiotherapy, targeted therapy, and immunotherapy, all presenting certain limitations such as pain, allergies, low immunity, superinfections, and amputations. To address these limitations, novel therapeutic approaches are required. Recent developments in terms of materials and fabrication strategies opened the door to the development of novel and promising strategies, which have been discussed in detail in this review. Additive manufacturing processes—mainly extrusion-based, powder bed fusion, and vat photopolymerization techniques—have been employed to process a wide range of materials (e.g., bioceramics, metals, and polymers) and produce synthetic implants for postoperative applications (Table 4). Different approaches were proposed focusing on the development of scaffolds made with advanced functional materials, anticancer drug-delivery scaffolds, and scaffolds for photothermal and magnetothermal applications. The design and fabrication of dual-functional scaffolds, discussed in this review in detail, represents an emerging area. Such scaffolds are designed to fulfil an initial treatment function, which can be achieved by incorporating specific drugs and materials exhibiting cytotoxicity at high concentrations or by applying NIR irradiation or a magnetic field that significantly increases the temperature in a localized region. After this initial therapeutic stage, the scaffold must be able to induce bone regeneration. Despite the initial stage of research, the

Table 4 Additive manufacturing techniques for various advanced cancer treatment strategies based on synthetic 3D scaffolds

Advanced cancer treatment strategy	Additive manufacturing technique	References
Scaffolds with advanced functional materials	Extrusion-based additive manufacturing	[119–121]
Drug-loaded scaffolds	Extrusion-based additive manufacturing	[138, 144, 146, 147]
	Laser-based powder bed fusion	[140–142, 148]
	Vat photopolymerization	[143]
	Melt-electrospinning	[139]
	Near-field electrospinning	[145]
Scaffolds for photothermal/magnetothermal therapy	Extrusion-based additive manufacturing	[149–158, 160–164]
	Laser-based powder bed fusion	[159]

Table 5 Limitations of the current materials [167–171]

Material	Limitations
Bioceramic	Limited mechanical properties due to inherent brittleness
	Difficult to control the degradation and resorption rate
	Difficult to process
Metal	Strong mechanical properties that can lead to stress-shielding
	Potential release of toxic ions
	High fabrication costs
Polymer	Potential pathological impurities (e.g., endotoxin) in natural polymers
	Possible inflammatory effects caused by acid degradation products
	Lack of cell recognition sites
	Limited mechanical properties
	Lack of bioactivity

results reported in this paper are highly promising, suggesting that this could be a highly relevant approach for bone cancer treatment applications. All of the reported approaches have shown great inhibition effects on both bone cancer cells (e.g., Saos-2 cells, MG-63 cells, MNNG/HOS cells, U_2OS cells, LM-8 cells, and K7M2wt cells) and other cancer cells with high bone metastasis risk (e.g., MDA-MB-231 cells, 4T1 cells, LAPC4 cells, ES-2-luc cells, and MIA PaCa-2 cells). Other bone cancer cell types, such as CADO-ES1, MHH-ES1, RD-ES, SK-ES-1 for Ewing sarcoma and SW-1353 for chondrosarcoma, should also be investigated in the future in this regard.

The reported biological studies (both in vitro and in vivo) correspond to short-term studies, which are insufficient to fully understand the behavior of these scaffolds. Therefore, long-term experiments are required to understand the effect of some reinforced materials such as graphene and GO, cancer recurrence, and the secondary effects associated with the incorporated drugs, degraded products, and ion release. Contrary to current studies that are limited to mice and rabbit models, large animal models should be implemented before human trials can commence.

As bone is a load-bearing tissue, the mechanical properties of the produced scaffolds are highly relevant to recovery. This is particularly critical for dual-functional scaffolds, which must support physiological loads during a significant period, gradually transferring the loads to the new bone formed during the regeneration phase. However, the commonly used materials present significant drawbacks regarding their mechanical properties. Polymers and ceramic materials present poor mechanical properties compared to bone tissue, while metals exhibit strong mechanical properties leading to stress shielding problems [165, 166]. Table 5 summarizes some of the inherent problems of the materials generally used in this field. Novel composite materials incorporating polymers, ceramics and low proportions of biodegradable metals (e.g., iron and zinc) should be investigated in the future to address these limitations.

The performance of the scaffolds discussed in this review is strongly linked to the addition of functional materials, loaded drugs, and photo-sensitizers or magneto-sensitizers. For local cancer treatment implants, the sustained and controllable release of drugs is crucial. However, it is challenging to precisely control the drug release kinetics using the approaches proposed to date [172]. In the case of scaffolds for photothermal/magnetothermal therapy, there is no systematic study or mathematical model correlating the materials (and material properties), heat release, and anticancer effects. These models are vital to design optimized scaffolds, and also to numerically predict their behavior, thus minimizing the need for animal studies. It is also essential to create models that allow the prediction of the number of anticancer drugs or photo-sensitizers or magneto-sensitizers to be used for a specific stage of cancer development, which could contribute to the advancement of stratified/personalized cancer treatment approaches.

Acknowledgements This research was partially supported by the Engineering and Physical Sciences Research Council (EPSRC) UK through the Global Challenges Research Fund (No. EP/R015139/1) and Rosetrees & Stoneygate Trust Enterprise Fellowship (Ref: A2750/M874) from Rosetrees Trust UK and Stoneygate Trust UK.

Author contributions YH was involved in conceptualization, investigation, writing—original draft, writing—review & editing, visualization; WW was involved in conceptualization, investigation, writing—review & editing, supervision, and funding acquisition; PB was involved in conceptualization, investigation, writing—review & editing, supervision, and funding acquisition.

Declarations

Conflict of interest The authors declare that they have no conflict of interest.

Ethical approval This article does not contain any studies with human or animal subjects performed by any of the authors.

References

1. All cancers fact. (2020) World Health Organization
2. Mariotto AB, Enewold L, Zhao J et al (2020) Medical care costs associated with cancer survivorship in the united states. Cancer Epidemiol Biomarkers Prev 29(7):1304–1312. https://doi.org/10.1158/1055-9965.EPI-19-1534
3. Hofmarcher T, Lindgren P, Wilking N et al (2020) The cost of cancer in Europe 2018. Eur J Cancer 129:41–49. https://doi.org/10.1016/j.ejca.2020.01.011
4. Van Driel M, Van Leeuwen JP (2014) Cancer and bone: a complex complex. Arch Biochem Biophys 561:159–166. https://doi.org/10.1016/j.abb.2014.07.013
5. Franchi A (2012) Epidemiology and classification of bone tumors. Clin Cases Miner Bone Metab 9(2):92–95
6. Kumar N, Gupta B (2016) Global incidence of primary malignant bone tumors. Curr Orthop Pract 27(5):530–534. https://doi.org/10.1097/Bco.0000000000000405
7. Brown HK, Schiavone K, Gouin F et al (2018) Biology of bone sarcomas and new therapeutic developments. Calcif Tissue Int 102(2):174–195. https://doi.org/10.1007/s00223-017-0372-2
8. Group EESNW (2012) Bone sarcomas: ESMO clinical practice guidelines for diagnosis, treatment and follow-up. Ann Oncol 23(Suppl 7):vii100–vii109. https://doi.org/10.1093/annonc/mds254
9. Harvey HA, Cream L (2007) Biology of bone metastases: causes and consequences. Clin Breast Cancer 7(Suppl):S7–S13. https://doi.org/10.3816/cbc.2007.s.001
10. Bumgardner JD, Chesnutt BM, Yuan Y et al (2007) The integration of chitosan-coated titanium in bone: an in vivo study in rabbits. Implant Dent 16(1):66–79. https://doi.org/10.1097/ID.0b013e3180312011
11. Hattori H, Masuoka K, Sato M et al (2006) Bone formation using human adipose tissue-derived stromal cells and a biodegradable scaffold. J Biomed Mater Res B 76b(1):230–239. https://doi.org/10.1002/jbm.b.30357
12. Gerrand C, Athanasou N, Brennan B et al (2016) UK guidelines for the management of bone sarcomas. Clin Sarcoma Res 6:7. https://doi.org/10.1186/s13569-016-0047-1
13. Makatsoris T, Kalofonos HP (2009) The role of chemotherapy in the treatment of bone metastases. Cancer Metastasis Biol Treat 12:287–298. https://doi.org/10.1007/978-1-4020-9819-2_14
14. Hanigan MH, Devarajan P (2003) Cisplatin nephrotoxicity: molecular mechanisms. Cancer Ther 1:47–61
15. Volkova M, Russell R 3rd (2011) Anthracycline cardiotoxicity: prevalence, pathogenesis and treatment. Curr Cardiol Rev 7(4):214–220. https://doi.org/10.2174/157340311799960645
16. Takemura G, Fujiwara H (2007) Doxorubicin-induced cardiomyopathy from the cardiotoxic mechanisms to management. Prog Cardiovasc Dis 49(5):330–352. https://doi.org/10.1016/j.pcad.2006.10.002
17. Kumar D, Kirshenbaum LA, Li T et al (2001) Apoptosis in adriamycin cardiomyopathy and its modulation by probucol. Antioxid Redox Signal 3(1):135–145. https://doi.org/10.1089/152308601750100641
18. Velasco R, Bruna J (2015) Taxane-induced peripheral neurotoxicity. Toxics 3(2):152–169. https://doi.org/10.3390/toxics3020152
19. Palumbo MO, Kavan P, Miller WH et al (2013) Systemic cancer therapy: achievements and challenges that lie ahead. Front Pharmacol 4:57. https://doi.org/10.3389/fphar.2013.00057
20. Anselmo AC, Mitragotri S (2016) Nanoparticles in the clinic. Bioeng Transl Med 1(1):10–29. https://doi.org/10.1002/btm2.10003
21. Rudnick-Glick S, Corem-Salkmon E, Grinberg I et al (2016) Targeted drug delivery of near IR fluorescent doxorubicin-conjugated poly(ethylene glycol) bisphosphonate nanoparticles for diagnosis and therapy of primary and metastatic bone cancer in a mouse model. J Nanobiotechnol 14(1):80. https://doi.org/10.1186/s12951-016-0233-6
22. Ahangar P, Akoury E, Ramirez Garcia Luna AS et al (2018) Nanoporous 3D-printed scaffolds for local doxorubicin delivery in bone metastases secondary to prostate cancer. Materials (Basel) 11(9):1485. https://doi.org/10.3390/ma11091485
23. Gardner DE, Mitchell DF, Mcdonald RE (1971) Treatment of pulps of monkeys with vancomycin and calcium hydroxide. J Dent Res 50(5):1273–1277. https://doi.org/10.1177/00220345710500053001
24. Stallmann HP, Faber C, Bronckers AL et al (2006) In vitro gentamicin release from commercially available calcium-phosphate bone substitutes influence of carrier type on duration of the release profile. BMC Musculoskelet Disord 7:18. https://doi.org/10.1186/1471-2474-7-18
25. Lee KY, Peters MC, Anderson KW et al (2000) Controlled growth factor release from synthetic extracellular matrices. Nature 408(6815):998–1000. https://doi.org/10.1038/35050141
26. Niu X, Feng Q, Wang M et al (2009) Porous nano-HA/collagen/PLLA scaffold containing chitosan microspheres for controlled delivery of synthetic peptide derived from BMP-2. J Contr Release 134(2):111–117. https://doi.org/10.1038/35050141
27. Lim SH, Kathuria H, Tan JJY et al (2018) 3D printed drug delivery and testing systems—a passing fad or the future? Adv Drug Del Rev 132:139–168. https://doi.org/10.1016/j.addr.2018.05.006
28. Hernigou P, Thiery JP, Benoit J et al (1989) Methotrexate diffusion from acrylic cement. Local chemotherapy for bone tumours. J Bone Joint Surg Br 71(5):804–811. https://doi.org/10.1302/0301-620X.71B5.2584251

29. Sun M, Wang M, Chen M et al (2015) A tissue-engineered therapeutic device inhibits tumor growth in vitro and in vivo. Acta Biomater 18:21–29. https://doi.org/10.1016/j.actbio.2015.02.004
30. Hutmacher DW, Sittinger M, Risbud MV (2004) Scaffold-based tissue engineering: Rationale for computer-aided design and solid free-form fabrication systems. Trends Biotechnol 22(7):354–362. https://doi.org/10.1016/j.tibtech.2004.05.005
31. Wei W, Zhang X, Zhang S et al (2019) Biomedical and bioactive engineered nanomaterials for targeted tumor photothermal therapy: a review. Mater Sci Eng C Mater Biol Appl 104:109891. https://doi.org/10.1016/j.msec.2019.109891
32. Ma H, Feng C, Chang J et al (2018) 3D-printed bioceramic scaffolds: From bone tissue engineering to tumor therapy. Acta Biomater 79:37–59. https://doi.org/10.1016/j.actbio.2018.08.026
33. Sarkar MR, Wachter N, Patka P et al (2001) First histological observations on the incorporation of a novel calcium phosphate bone substitute material in human cancellous bone. J Biomed Mater Res 58(3):329–334. https://doi.org/10.1002/1097-4636(2001)58:3%3c329::aid-jbm1025%3e3.0.co;2-9
34. Madanagopal TT, Agarwalla SV, Rosa V (2019) 3—Carbon nanocomposites for implant dentistry and bone tissue engineering. In: Applications of nanocomposite materials in dentistry. Woodhead Publishing, pp 47–63. https://doi.org/10.1016/B978-0-12-813742-0.00003-1
35. Langton CM, Njeh CF (2016) The physical measurement of bone. CRC Press, Boca Raton
36. Arnett T (2016) Bone structure and function: organization & composition of bone, bone modelling and remodelling, bone cells. In: 43rd Annual european calcified tissue society congress. BioScientifica. https://doi.org/10.1530/boneabs.5.AHP1.1
37. Gonzalez Diaz EC, Sinha S, Avedian RS et al (2019) Tissue-engineered 3D models for elucidating primary and metastatic bone cancer progression. Acta Biomater 99:18–32. https://doi.org/10.1016/j.actbio.2019.08.020
38. Fletcher CDM, Hogendoorn P, Mertens F (2013) WHO classification of tumors of soft tissue and bone. IARC Press, Lyon, pp 321–324
39. Perrin W (2014) Osteosarcoma information for patients. Oxford University Hospitals NHS Trust.
40. Whelan JS, Jinks RC, Mctiernan A et al (2012) Survival from high-grade localised extremity osteosarcoma: combined results and prognostic factors from three European osteosarcoma intergroup randomised controlled trials. Ann Oncol 23(6):1607–1616. https://doi.org/10.1093/annonc/mdr491
41. Dennis N, Francis M, Lawrence G (2012) Bone sarcoma incidence and survival. Tumours diagnosed between 1985 and 2009. National Cancer Intelligence Network
42. Freeman AK, Sumathi VP, Jeys L (2015) Primary malignant tumours of the bone. Surg Infect (Larchmt) 33(1):26–33. https://doi.org/10.1016/j.mpsur.2014.10.006
43. Mirabello L, Troisi RJ, Savage SA (2009) Osteosarcoma incidence and survival rates from 1973 to 2004: data from the surveillance, epidemiology, and end results program. Cancer 115(7):1531–1543. https://doi.org/10.1002/cncr.24121
44. Freeman AK, Sumathi VP, Jeys L (2018) Primary malignant tumours of the bone. Surg Infect (Larchmt) 36(1):27–34. https://doi.org/10.1016/j.mpsur.2017.10.001
45. Paulussen M, Bielack S, Jürgens H et al (2009) Ewing's sarcoma of the bone: ESMO clinical recommendations for diagnosis, treatment and follow-up. Ann Oncol 20(Suppl 4):140–142. https://doi.org/10.1093/annonc/mdp155
46. Grimer R, Athanasou N, Gerrand C et al (2010) UK guidelines for the management of bone sarcomas. Sarcoma 2010:317462. https://doi.org/10.1155/2010/317462
47. Cotterill SJ, Ahrens S, Paulussen M et al (2000) Prognostic factors in Ewing's tumor of bone: analysis of 975 patients from the European intergroup cooperative Ewing's sarcoma study group. J Clin Oncol 18(17):3108–3114. https://doi.org/10.1200/jco.2000.18.17.3108
48. Bernstein M, Kovar H, Paulussen M et al (2006) Ewing's sarcoma family of tumors: current management. Oncologist 11(5):503–519. https://doi.org/10.1634/theoncologist.11-5-503
49. Delattre O, Zucman J, Melot T et al (1994) The Ewing family of tumors-a subgroup of small-round-cell tumors defined by specific chimeric transcripts. N Engl J Med 331(5):294–299. https://doi.org/10.1056/NEJM199408043310503
50. Verdegaal SH, Bovee JV, Pansuriya TC et al (2011) Incidence, predictive factors, and prognosis of chondrosarcoma in patients with ollier disease and maffucci syndrome: an international multicenter study of 161 patients. Oncologist 16(12):1771–1779. https://doi.org/10.1634/theoncologist.2011-0200
51. Macedo F, Ladeira K, Pinho F et al (2017) Bone metastases: an overview. Oncol Rev 11(1):321. https://doi.org/10.4081/oncol.2017.321
52. Cecchini MG, Wetterwald A, van der Pluijm G et al (2005) Molecular and biological mechanisms of bone metastasis. EAU Updat Ser 3(4):214–226. https://doi.org/10.1016/j.euus.2005.09.006
53. Chambers AF, Naumov GN, Varghese HJ et al (2001) Critical steps in hematogenous metastasis: an overview. Surg Oncol Clin N Am 10(2):243–255
54. Luzzi KJ, Macdonald IC, Schmidt EE et al (1998) Multistep nature of metastatic inefficiency: dormancy of solitary cells after successful extravasation and limited survival of early micrometastases. Am J Pathol 153(3):865–873. https://doi.org/10.1016/S0002-9440(10)65628-3
55. Selvaggi G, Scagliotti GV (2005) Management of bone metastases in cancer: a review. Crit Rev Oncol Hematol 56(3):365–378. https://doi.org/10.1016/j.critrevonc.2005.03.011
56. Chiechi A, Guise TA (2016) Pathobiology of osteolytic and osteoblastic bone metastases. In: Randall RL (ed) Metastatic bone disease: an integrated approach to patient care. Springer, New York, pp 15–35. https://doi.org/10.1007/978-1-4614-5662-9_2
57. Zhang Y, Rosenberg AE (2017) Bone-forming tumors. Surg Pathol Clin 10(3):513–535. https://doi.org/10.1016/j.path.2017.04.006
58. Hakim DN, Pelly T, Kulendran M et al (2015) Benign tumours of the bone: a review. J Bone Oncol 4(2):37–41. https://doi.org/10.1016/j.jbo.2015.02.001
59. Sobti A, Agrawal P, Agarwala S et al (2016) Giant cell tumor of bone-an overview. Arch Bone Jt Surg 4(1):2–9
60. Casimiro S, Guise TA, Chirgwin J (2009) The critical role of the bone microenvironment in cancer metastases. Mol Cell Endocrinol 310(1–2):71–81. https://doi.org/10.1016/j.mce.2009.07.004
61. Hauschka PV, Mavrakos AE, Iafrati MD et al (1986) Growth factors in bone matrix. Isolation of multiple types by affinity chromatography on heparin-sepharose. J Biol Chem 261(27):12665–12674
62. Clines GA, Guise TA (2005) Hypercalcaemia of malignancy and basic research on mechanisms responsible for osteolytic and osteoblastic metastasis to bone. Endocr Relat Cancer 12(3):549–583. https://doi.org/10.1677/erc.1.00543
63. Charhon SA, Chapuy MC, Delvin EE et al (1983) Histomorphometric analysis of sclerotic bone metastases from prostatic carcinoma special reference to osteomalacia. Cancer 51(5):918–924. https://doi.org/10.1002/1097-0142(19830301)51:5%3c918::aid-cncr2820510526%3e3.0.co;2-j
64. Koutsilieris M (1995) Skeletal metastases in advanced prostate cancer: cell biology and therapy. Crit Rev Oncol Hematol 18(1):51–64. https://doi.org/10.1016/1040-8428(94)00122-a

65. Treating Bone Metastasis (2021) WebMD. https://www.webmd.com/cancer/treating-bone-metastasis-breast-cancer. Accessed 1 July 2021
66. Canal C, Fontelo R, Hamouda I et al (2017) Plasma-induced selectivity in bone cancer cells death. Free Radic Biol Med 110:72–80. https://doi.org/10.1016/j.freeradbiomed.2017.05.023
67. Bone Cancer Treatment (2021) National Health Service. https://www.nhs.uk/conditions/bone-cancer/treatment/. Accessed 1 July 2021
68. Rose PS, Clarke MJ, Dekutoski MB (2011) Minimally invasive treatment of spinal metastases: Techniques. Int J Surg Oncol 2011:494381. https://doi.org/10.1155/2011/494381
69. Wittig JC, Bickels J, Priebat D et al (2002) Osteosarcoma: a multidisciplinary approach to diagnosis and treatment. Am Fam Physician 65(6):1123–1132
70. Enneking WF, Spanier SS, Goodman MA (1980) A system for the surgical staging of musculoskeletal sarcoma. Clin Orthop Relat Res 153:106–120
71. Bacci G, Forni C, Longhi A et al (2007) Local recurrence and local control of non-metastatic osteosarcoma of the extremities: a 27-year experience in a single institution. J Surg Oncol 96(2):118–123. https://doi.org/10.1002/jso.20628
72. Enneking WF, Spanier SS, Malawer MM (1981) The effect of the anatomic setting on the results of surgical procedures for soft parts sarcoma of the thigh. Cancer 47(5):1005–1022. https://doi.org/10.1002/1097-0142(19810301)47:5%3c1005::aid-cncr2820470532%3e3.0.co;2-9
73. Steele KH, Raurell A, Ashford RU (2017) Surgical management of soft tissue sarcoma. Orthop Trauma 31(3):180–187. https://doi.org/10.1016/j.mporth.2017.03.012
74. Schoenfeld AJ, Hornicek FJ, Pedlow FX et al (2010) Osteosarcoma of the spine: experience in 26 patients treated at the massachusetts general hospital. Spine J 10(8):708–714. https://doi.org/10.1016/j.spinee.2010.05.017
75. Grimer RJ, Carter SR, Pynsent PB (1997) The cost-effectiveness of limb salvage for bone tumours. J Bone Joint Surg Br 79b(4):558–561. https://doi.org/10.1302/0301-620x.79b4.7687
76. Henderson ER, O'connor MI, Ruggieri P et al (2014) Classification of failure of limb salvage after reconstructive surgery for bone tumours: a modified system including biological and expandable reconstructions. Bone Joint J 96-B(11):1436–1440. https://doi.org/10.1302/0301-620X.96B11.34747
77. Carrle D, Bielack SS (2006) Current strategies of chemotherapy in osteosarcoma. Int Orthop 30(6):445–451. https://doi.org/10.1007/s00264-006-0192-x
78. Dickens E, Ahmed S (2021) Principles of cancer treatment by chemotherapy. Surg Infect (Larchmt) 39(4):215–220. https://doi.org/10.1016/j.mpsur.2021.01.009
79. Anninga JK, Gelderblom H, Fiocco M et al (2011) Chemotherapeutic adjuvant treatment for osteosarcoma: where do we stand? Eur J Cancer 47(16):2431–2445. https://doi.org/10.1016/j.ejca.2011.05.030
80. Gutowski CJ, Basu-Mallick A, Abraham JA (2016) Management of bone sarcoma. Surg Clin N Am 96(5):1077–1106. https://doi.org/10.1016/j.suc.2016.06.002
81. Ragupathi G, Meyers M, Adluri S et al (2000) Induction of antibodies against GD3 ganglioside in melanoma patients by vaccination with GD3-lactone-klh conjugate plus immunological adjuvant QS-21. Int J Cancer 85(5):659–666. https://doi.org/10.1002/(sici)1097-0215(20000301)85:5%3c659::Aid-ijc11%3e3.0.Co;2-5
82. He YC, Chen JW, Cao J et al (2003) Toxicities and therapeutic effect of 5-fluorouracil controlled release implant on tumor-bearing rats. World J Gastroenterol 9(8):1795–1798. https://doi.org/10.3748/wjg.v9.i8.1795
83. Curnis F, Sacchi A, Corti A (2002) Improving chemotherapeutic drug penetration in tumors by vascular targeting and barrier alteration. J Clin Invest 110(4):475–482. https://doi.org/10.1172/JCI15223
84. Schlemmer HP, Becker M, Bachert P et al (1999) Alterations of intratumoral pharmacokinetics of 5-fluorouracil in head and neck carcinoma during simultaneous radiochemotherapy. Cancer Res 59(10):2363–2369
85. Goldberg EP, Hadba AR, Almond BA et al (2002) Intratumoral cancer chemotherapy and immunotherapy: Opportunities for nonsystemic preoperative drug delivery. J Pharm Pharmacol 54(2):159–180. https://doi.org/10.1211/0022357021778268
86. Dreher MR, Liu W, Michelich CR et al (2006) Tumor vascular permeability, accumulation, and penetration of macromolecular drug carriers. J Natl Cancer Inst 98(5):335–344. https://doi.org/10.1093/jnci/djj070
87. Imai R, Kamada T, Araki N et al (2016) Carbon ion radiation therapy for unresectable sacral chordoma: an analysis of 188 cases. Int J Radiat Oncol Biol Phys 95(1):322–327. https://doi.org/10.1016/j.ijrobp.2016.02.012
88. Baumann BC, Lustig RA, Mazzoni S et al (2015) A prospective clinical trial of proton therapy for chordoma and chondrosarcoma. Int J Radiat Oncol 93(3):E641. https://doi.org/10.1016/j.ijrobp.2015.07.2184
89. Sole CV, Calvo FA, Polo A et al (2015) Intraoperative electron-beam radiation therapy for pediatric Ewing sarcomas and rhabdomyosarcomas: long-term outcomes. Int J Radiat Oncol Biol Phys 92(5):1069–1076. https://doi.org/10.1016/j.ijrobp.2015.04.048
90. Vaidya JS (2021) Principles of cancer treatment by radiotherapy. Surg Infect (Larchmt) 39(4):193–201. https://doi.org/10.1016/j.mpsur.2021.02.002
91. Berrington De Gonzalez A, Kutsenko A, Rajaraman P (2012) Sarcoma risk after radiation exposure. Clin Sarcoma Res 2(1):18. https://doi.org/10.1186/2045-3329-2-18
92. Gladdy RA, Qin LX, Moraco N et al (2010) Do radiation-associated soft tissue sarcomas have the same prognosis as sporadic soft tissue sarcomas? J Clin Oncol 28(12):2064–2069. https://doi.org/10.1200/Jco.2009.25.1728
93. Jamil N, Howie S, Salter DM (2010) Therapeutic molecular targets in human chondrosarcoma. Int J Exp Pathol 91(5):387–393. https://doi.org/10.1111/j.1365-2613.2010.00749.x
94. Bovee JV, Cleton-Jansen AM, Taminiau AH et al (2005) Emerging pathways in the development of chondrosarcoma of bone and implications for targeted treatment. Lancet Oncol 6(8):599–607. https://doi.org/10.1016/S1470-2045(05)70282-5
95. Jayson GC, Kerbel R, Ellis LM et al (2016) Antiangiogenic therapy in oncology: current status and future directions. Lancet 388(10043):518–529. https://doi.org/10.1016/S0140-6736(15)01088-0
96. Lebellec L, Chauffert B, Blay JY et al (2017) Advanced chordoma treated by first-line molecular targeted therapies: Outcomes and prognostic factors. A retrospective study of the french sarcoma group (GSF/GETO) and the association des neuro-oncologues d'expression francaise (ANOCEF). Eur J Cancer 79:119–128. https://doi.org/10.1016/j.ejca.2017.03.037
97. Coleman RE (2012) Adjuvant bone-targeted therapy to prevent metastasis: lessons from the azure study. Curr Opin Support Palliat Care 6(3):322–329. https://doi.org/10.1097/SPC.0b013e32835689cd
98. Onishi T, Hayashi N, Theriault RL et al (2010) Future directions of bone-targeted therapy for metastatic breast cancer. Nat Rev Clin Oncol 7(11):641–651. https://doi.org/10.1038/nrclinonc.2010.134

99. Rajan S, Cam M, Gross AC, et al (2020) Osteosarcoma tumors maintain intratumoral heterogeneity, even while adapting to environmental pressures that drive clonal selection. https://doi.org/10.1101/2020.11.03.367342
100. Futakuchi M, Fukamachi K, Suzui M (2016) Heterogeneity of tumor cells in the bone microenvironment: Mechanisms and therapeutic targets for bone metastasis of prostate or breast cancer. Adv Drug Deliv Rev 99(PtB):206–211. https://doi.org/10.1016/j.addr.2015.11.017
101. Targeted cancer drugs for bone cancer (2021) Cancer Research UK. https://www.cancerresearchuk.org/about-cancer/bone-cancer/treatment/Targeted-cancer-drugs. Accessed 1 July 2021
102. Ventola CL (2017) Cancer immunotherapy, part 2: efficacy, safety, and other clinical considerations. Pharm Thr 42(7):452–463
103. Nathenson MJ, Conley AP, Sausville E (2018) Immunotherapy: a new (and old) approach to treatment of soft tissue and bone sarcomas. Oncologist 23(1):71–83. https://doi.org/10.1634/theoncologist.2016-0025
104. Uehara T, Fujiwara T, Takeda K et al (2015) Immunotherapy for bone and soft tissue sarcomas. Biomed Res Int 2015:820813. https://doi.org/10.1155/2015/820813
105. Marcove RC, Southam CM, Levin A et al (1971) A clinical trial of autogenous vaccine in osteogenic sarcoma in patients under the age of twenty-five. Surg Forum 22:434–435
106. Rosenberg SA, Yang JC, Restifo NP (2004) Cancer immunotherapy: moving beyond current vaccines. Nat Med 10(9):909–915. https://doi.org/10.1038/nm1100
107. Maki RG (2006) Future directions for immunotherapeutic intervention against sarcomas. Curr Opin Oncol 18(4):363–368. https://doi.org/10.1097/01.cco.0000228743.72165.86
108. Vergati M, Intrivici C, Huen NY et al (2010) Strategies for cancer vaccine development. J Biomed Biotechnol 2010:596432. https://doi.org/10.1155/2010/596432
109. Dudley ME, Rosenberg SA (2003) Adoptive-cell-transfer therapy for the treatment of patients with cancer. Nat Rev Cancer 3(9):666–675. https://doi.org/10.1038/nrc1167
110. Pardoll DM (2012) Immunology beats cancer: a blueprint for successful translation. Nat Immunol 13(12):1129–1132. https://doi.org/10.1038/ni.2392
111. Lee S, Margolin K (2011) Cytokines in cancer immunotherapy. Cancers (Basel) 3(4):3856–3893. https://doi.org/10.3390/cancers3043856
112. Ogihara Y, Takeda K, Yanagawa T et al (1994) Spontaneous regression of lung metastases from osteosarcoma. Cancer 74(10):2798–2803. https://doi.org/10.1002/1097-0142(19941115)74:10%3c2798::Aid-cncr2820741009%3e3.0.Co;2-2
113. Sabate JM, Llauger J, Torrubia S et al (1998) Osteosarcoma of the abdominal wall with spontaneous regression of lung metastases. AJR Am J Roentgenol 171(3):691–692. https://doi.org/10.2214/ajr.171.3.9725297
114. Nabeta Y, Kawaguchi S, Sahara H et al (2003) Recognition by cellular and humoral autologous immunity in a human osteosarcoma cell line. J Orthop Sci 8(4):554–559. https://doi.org/10.1007/s00776-003-0663-5
115. Slovin SF, Lackman RD, Ferrone S et al (1986) Cellular immune response to human sarcomas: cytotoxic t cell clones reactive with autologous sarcomas. I. Development, phenotype, and specificity. J Immunol 137(9):3042–3048
116. Sato Y, Nabeta Y, Tsukahara T et al (2002) Detection and induction of CTLs specific for syt-ssx-derived peptides in HLA-A24^{+} patients with synovial sarcoma. J Immunol 169(3):1611–1618. https://doi.org/10.4049/jimmunol.169.3.1611
117. Worley BS, Van Den Broeke LT, Goletz TJ et al (2001) Antigenicity of fusion proteins from sarcoma-associated chromosomal translocations. Cancer Res 61(18):6868–6875
118. Heymann MF, Schiavone K, Heymann D (2021) Bone sarcomas in the immunotherapy era. Br J Pharmacol 178(9):1955–1972. https://doi.org/10.1111/bph.14999
119. Hou Y, Wang W, Bartolo PJDS (2020) Investigating the effect of carbon nanomaterials reinforcing ooly (ε-caprolactone) printed scaffolds for bone repair applications. Int J Bioprint 6(2):266. https://doi.org/10.18063/ijb.v6i2.266
120. Hou YH, Wang WG, Bartolo P (2020) Novel poly(e-caprolactone)/graphene scaffolds for bone cancer treatment and bone regeneration. 3D Print Addit Manuf 7(5):222–229. https://doi.org/10.1089/3dp.2020.0051
121. Zhu SS, Yao LY, Pan CL et al (2021) 3D printed gellan gum/graphene oxide scaffold for tumor therapy and bone reconstruction. Comp Sci Technol 208:108763. https://doi.org/10.1016/j.compscitech.2021.108763
122. Hu M, Fang J, Zhang Y et al (2020) Design and evaluation a kind of functional biomaterial for bone tissue engineering: Selenium/mesoporous bioactive glass nanospheres. J Colloid Interface Sci 579:654–666. https://doi.org/10.1016/j.jcis.2020.06.122
123. Wang X, Zhang Y, Ma Y et al (2016) Selenium - containing mesoporous bioactive glass particles: Physicochemical and drug delivery properties. Ceram Int 42(2):3609–3617. https://doi.org/10.1016/j.ceramint.2015.11.024
124. Sarin N, Singh KJ, Singh D et al (2020) Preliminary studies of strontium and selenium binary doped CaO-SiO_2-P_2O_5-MgO bioceramics for faster growth of hydroxyapatite and bone regeneration applications. Mater Chem Phys 253:123329. https://doi.org/10.1016/j.matchemphys.2020.123329
125. Wang Y, Wang J, Hao H et al (2016) In vitro and in vivo mechanism of bone tumor inhibition by selenium-doped bone mineral nanoparticles. ACS Nano 10(11):9927–9937. https://doi.org/10.1021/acsnano.6b03835
126. Li X, Wang Y, Chen Y et al (2020) Hierarchically constructed selenium-doped bone-mimetic nanoparticles promote ROS-mediated autophagy and apoptosis for bone tumor inhibition. Biomaterials 257:120253. https://doi.org/10.1016/j.biomaterials.2020.120253
127. Zhao P, Li M, Chen Y et al (2019) Selenium-doped calcium carbonate nanoparticles loaded with cisplatin enhance efficiency and reduce side effects. Int J Pharm 570:118638. https://doi.org/10.1016/j.ijpharm.2019.118638
128. He L, Li HY, Chen XY et al (2019) Selenium-substituted hydroxyapatite particles with regulated microstructures for osteogenic differentiation and anti-tumor effects. Ceram Int 45(11):13787–13798. https://doi.org/10.1016/j.ceramint.2019.04.075
129. Barbanente A, Nadar RA, Degli Esposti L et al (2020) Platinum-loaded, selenium-doped hydroxyapatite nanoparticles selectively reduce proliferation of prostate and breast cancer cells co-cultured in the presence of stem cells. J Mater Chem B 8(14):2792–2804. https://doi.org/10.1039/d0tb00390e
130. Khan S, Ullah MW, Siddique R et al (2019) Catechins-modified selenium-doped hydroxyapatite nanomaterials for improved osteosarcoma therapy through generation of reactive oxygen species. Front Oncol 9:499. https://doi.org/10.3389/fonc.2019.00499
131. Barbanente A, Palazzo B, Esposti LD et al (2021) Selenium-doped hydroxyapatite nanoparticles for potential application in bone tumor therapy. J Inorg Biochem 215:111334. https://doi.org/10.1016/j.jinorgbio.2020.111334
132. Zhou JH, Wang XL (2020) The osteogenic, anti-oncogenic and antibacterial activities of selenium-doped titanium dioxide coatings on titanium. Surf Coat Tech 403:126408. https://doi.org/10.1016/j.surfcoat.2020.126408
133. Chen XY, Cai KY, Fang JJ et al (2013) Fabrication of selenium-deposited and chitosan-coated titania nanotubes with anticancer

and antibacterial properties. Colloid Surface B 103:149–157. https://doi.org/10.1016/j.colsurfb.2012.10.022
134. Tran PA, Sarin L, Hurt RH et al (2010) Titanium surfaces with adherent selenium nanoclusters as a novel anticancer orthopedic material. J Biomed Mater Res Part A 93a(4):1417–1428. https://doi.org/10.1002/jbm.a.32631
135. Stolzoff M, Webster TJ (2016) Reducing bone cancer cell functions using selenium nanocomposites. J Biomed Mater Res Part A 104(2):476–482. https://doi.org/10.1002/jbm.a.35583
136. Karahaliloglu Z, Kilicay E (2020) In vitro evaluation of bone cements impregnated with selenium nanoparticles stabilized by phosphatidylcholine (PC) for application in bone. J Biomater Appl 35(3):385–404. https://doi.org/10.1177/0885328220933781
137. Filipovic N, Veselinovic L, Razic S et al (2019) Poly (epsilon-caprolactone) microspheres for prolonged release of selenium nanoparticles. Mat Sci Eng C Mater 96:776–789. https://doi.org/10.1016/j.msec.2018.11.073
138. Chen M, Le DQ, Hein S et al (2012) Fabrication and characterization of a rapid prototyped tissue engineering scaffold with embedded multicomponent matrix for controlled drug release. Int J Nanomed 7:4285–4297. https://doi.org/10.2147/IJN.S33083
139. Lahr CA, Landgraf M, Sanchez-Herrero A et al (2020) A 3D-printed biomaterials-based platform to advance established therapy avenues against primary bone cancers. Acta Biomater 118:69–82. https://doi.org/10.1016/j.actbio.2020.10.006
140. Salmoria GV, Vieira FE, Ghizoni GB et al (2017) Additive manufacturing of PE/fluorouracil waffles for implantable drug delivery in bone cancer treatment. Inter J Eng Res Sci 3(6):62–70
141. Salmoria GV, Vieira F, Ghizoni G et al (2017) 3D printing of PCL/fluorouracil tablets by selective laser sintering: properties of implantable drug delivery for cartilage cancer treatment. Drugs 4:6
142. Salmoria GV, Vieira FE, Muenz EA et al (2018) Additive manufacturing of PE/fluorouracil/progesterone intrauterine device for endometrial and ovarian cancer treatments. Polym Test 71:312–317. https://doi.org/10.1016/j.polymertesting.2018.09.023
143. Wang YH, Sun L, Mei ZG et al (2020) 3D printed biodegradable implants as an individualized drug delivery system for local chemotherapy of osteosarcoma. Mater Des 186:108336. https://doi.org/10.1016/j.matdes.2019.108336
144. Yi HG, Choi YJ, Kang KS et al (2016) A 3D-printed local drug delivery patch for pancreatic cancer growth suppression. J Controll Rel 238:231–241. https://doi.org/10.1016/j.jconrel.2016.06.015
145. Yang Y, Qiao X, Huang R et al (2020) E-jet 3D printed drug delivery implants to inhibit growth and metastasis of orthotopic breast cancer. Biomaterials 230:119618. https://doi.org/10.1016/j.biomaterials.2019.119618
146. Cho H, Jammalamadaka U, Tappa K et al (2019) 3D printing of poloxamer 407 nanogel discs and their applications in adjuvant ovarian cancer therapy. Mol Pharm 16(2):552–560. https://doi.org/10.1021/acs.molpharmaceut.8b00836
147. Hoang Phuc D, Shafiee A, Lahr CA et al (2020) Local doxorubicin delivery via 3D-printed porous scaffolds reduces systemic cytotoxicity and breast cancer recurrence in mice. Adv Ther 3(9):2000056. https://doi.org/10.1002/adtp.202000056
148. Maher S, Kaur G, Lima-Marques L et al (2017) Engineering of micro- to nanostructured 3D-printed drug-releasing titanium implants for enhanced osseointegration and localized delivery of anticancer drugs. ACS Appl Mater Interf 9(35):29562–29570. https://doi.org/10.1021/acsami.7b09916
149. Zhang J, Zhao S, Zhu M et al (2014) 3D-printed magnetic Fe_3O_4/MBG/PCL composite scaffolds with multifunctionality of bone regeneration, local anticancer drug delivery and hyperthermia. J Mater Chem B 2(43):7583–7595. https://doi.org/10.1039/c4tb01063a
150. Dong S, Chen Y, Yu L et al (2020) Magnetic hyperthermia-synergistic H_2O_2 self-sufficient catalytic suppression of osteosarcoma with enhanced bone-regeneration bioactivity by 3D-printing composite scaffolds. Adv Funct Mater 30(4):1907071. https://doi.org/10.1002/adfm.201907071
151. Wang XC, Li T, Ma HS et al (2017) A 3D-printed scaffold with MoS_2 nanosheets for tumor therapy and tissue regeneration. NPG Asia Mater 9:e376. https://doi.org/10.1038/am.2017.47
152. Zhuang H, Lin R, Liu Y et al (2019) Three-dimensional-printed bioceramic scaffolds with osteogenic activity for simultaneous photo/magnetothermal therapy of bone tumors. ACS Biomater Sci Eng 5(12):6725–6734. https://doi.org/10.1021/acsbiomaterials.9b01095
153. Yang Q, Yin H, Xu T et al (2020) Engineering 2D mesoporous silica@MXene-integrated 3D-printing scaffolds for combinatory osteosarcoma therapy and NO-augmented bone regeneration. Small 16(14):1906814. https://doi.org/10.1002/smll.201906814
154. Pan S, Yin J, Yu L et al (2020) 2D mxene-integrated 3D-printing scaffolds for augmented osteosarcoma phototherapy and accelerated tissue reconstruction. Adv Sci 7(2):1901511. https://doi.org/10.1002/advs.201901511
155. Wang H, Zeng XQ, Pang LB et al (2020) Integrative treatment of anti-tumor/bone repair by combination of MoS_2 nanosheets with 3D printed bioactive borosilicate glass scaffolds. Chem Eng J 396:125081. https://doi.org/10.1016/j.cej.2020.125081
156. Dang W, Li T, Li B et al (2018) A bifunctional scaffold with $CuFeSe_2$ nanocrystals for tumor therapy and bone reconstruction. Biomaterials 160:92–106. https://doi.org/10.1016/j.biomaterials.2017.11.020
157. Dang WT, Jin YY, Yi K et al (2021) Hemin particles-functionalized 3D printed scaffolds for combined photothermal and chemotherapy of osteosarcoma. Chem Eng J 422:129919. https://doi.org/10.1016/j.cej.2021.129919
158. Liu YQ, Li T, Ma HS et al (2018) 3D-printed scaffolds with bioactive elements-induced photothermal effect for bone tumor therapy. Acta Biomater 73:531–546. https://doi.org/10.1016/j.actbio.2018.04.014
159. Ma HS, Li T, Huan ZG et al (2018) 3D printing of high-strength bioscaffolds for the synergistic treatment of bone cancer. NPG Asia Mater 10:31–44. https://doi.org/10.1038/s41427-018-0015-8
160. Fu SY, Hu HR, Chen JJ et al (2020) Silicone resin derived larnite/C scaffolds via 3D printing for potential tumor therapy and bone regeneration. Chem Eng J 382:122928. https://doi.org/10.1016/j.cej.2019.122928
161. Ma HS, Luo J, Sun Z et al (2016) 3D printing of biomaterials with mussel-inspired nanostructures for tumor therapy and tissue regeneration. Biomaterials 111:138–148. https://doi.org/10.1016/j.biomaterials.2016.10.005
162. Ma H, Jiang C, Zhai D et al (2016) A bifunctional biomaterial with photothermal effect fortumor therapy and bone regeneration. Adv Funct Mater 26(8):1197–1208. https://doi.org/10.1002/adfm.201504142
163. Dong S, Zhang YN, Wan J et al (2020) A novel multifunctional carbon aerogel-coated platform for osteosarcoma therapy and enhanced bone regeneration. J Mater Chem B 8(3):368–379. https://doi.org/10.1039/c9tb02383f
164. Dang WT, Ma B, Huan ZG et al (2019) LaB_6 surface chemistry-reinforced scaffolds for treating bone tumors and bone defects. Appl Mater Today 16:42–55. https://doi.org/10.1016/j.apmt.2019.04.015

165. Al-Tamimi AA, Huang BY, Vyas C et al (2019) Topology optimised metallic bone plates produced by electron beam melting: a mechanical and biological study. Int J Adv Manuf Tech 104(1–4):195–210. https://doi.org/10.1007/s00170-019-03866-0
166. Al-Tamimi AA, Hernandez MA, Omar A et al (2020) Mechanical, biological and tribological behaviour of fixation plates 3D printed by electron beam and selective laser melting. Int J Adv Manuf Tech 109(3–4):673–688. https://doi.org/10.1007/s00170-020-05676-1
167. Kanczler JM, Wells JA, Gibbs DMR et al (2020) Chapter 50-bone tissue engineering and bone regeneration. In: Principles of tissue engineering, 5th edn. Academic Press, pp 917–935. https://doi.org/10.1016/B978-0-12-818422-6.00052-6
168. Thavornyutikarn B, Chantarapanich N, Sitthiseripratip K et al (2014) Bone tissue engineering scaffolding: computer-aided scaffolding techniques. Prog Biomater 3:61–102. https://doi.org/10.1007/s40204-014-0026-7
169. Turnbull G, Clarke J, Picard F et al (2018) 3D bioactive composite scaffolds for bone tissue engineering. Bioact Mater 3(3):278–314. https://doi.org/10.1016/j.bioactmat.2017.10.001
170. Kalsi S, Singh J, Sehgal SS et al (2021) Biomaterials for tissue engineered bone scaffolds: a review. Mate Today Proc. https://doi.org/10.1016/j.matpr.2021.04.273
171. Koons GL, Diba M, Mikos AG (2020) Materials design for bone-tissue engineering. Nat Rev Mater 5(8):584–603. https://doi.org/10.1038/s41578-020-0204-2
172. Habraken WJEM, Wolke JGC, Jansen JA (2007) Ceramic composites as matrices and scaffolds for drug delivery in tissue engineering. Adv Drug Del Rev 59(4–5):234–248. https://doi.org/10.1016/j.addr.2007.03.011